Article

Cell Reports

Viral-Mediated AURKB Cleavage Promotes Cell Segregation and Tumorigenesis

Graphical Abstract

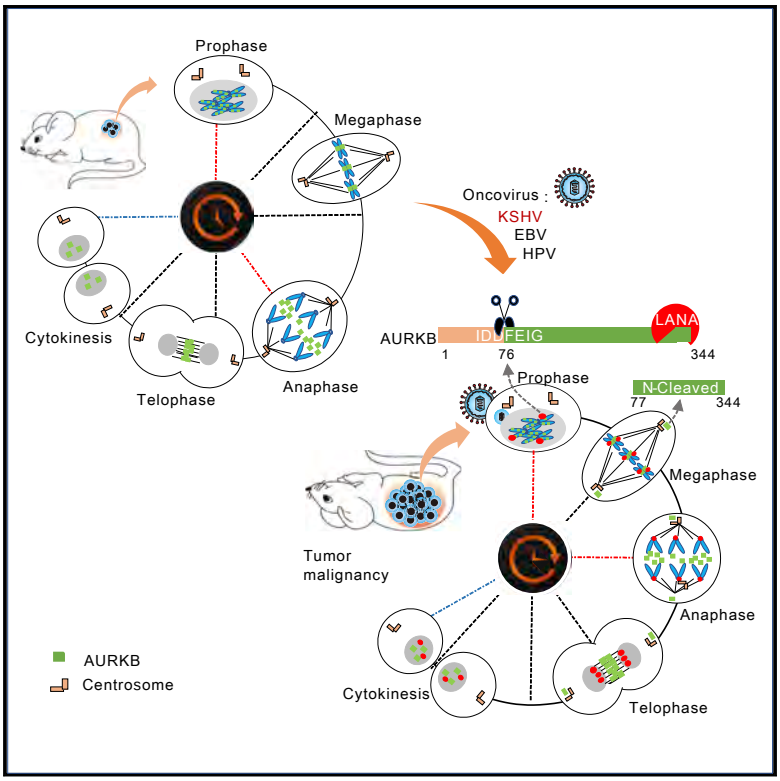

Authors

Qing Zhu, Ling Ding, Zhenguo Zi, ..., Zhenghong Yuan, Fang Wei, Qiliang Cai

Correspondence

qiliang@fudan.edu.cn

In Brief

Zhu et al. find that proteolytic cleavage of AURKB occurs in several oncovirus-associated cancer cells. Specifically, the oncovirus antigen LANA cleaves AURKB to promote the metaphase-to-telophase transition, thereby inducing host cell segregation and tumorigenesis.

Highlights

- Cleaved AURKB exists in many oncovirus-related cancer cells and patient cancer tissue
- Oncovirus-mediated AURKB cleavage occurs at Asp^{76} and relies on a serine protease
- The N′-AURKB promotes the metaphase-to-telophase transition in mitotic cells
- The N′-AURKB promotes tumor growth and malignancy *in vitro* and *in vivo*

Zhu et al., 2019, Cell Reports *26*, 3657–3671
March 26, 2019
https://doi.org/10.1016/j.celrep.2019.02.106

CellPress

Cell Reports
Article

Viral-Mediated AURKB Cleavage Promotes Cell Segregation and Tumorigenesis

Qing Zhu,[1,5] Ling Ding,[1,5] Zhenguo Zi,[3,5] Shujun Gao,[4,5] Chong Wang,[1] Yuyan Wang,[1] Caixia Zhu,[1] Zhenghong Yuan,[1] Fang Wei,[3] and Qiliang Cai[1,2,6,*]

[1]MOE and MOH Key Laboratory of Medical Molecular Virology, School of Basic Medicine, Shanghai Medical College, Fudan University, Shanghai 200032, China

[2]Expert Workstation, Baoji Central Hospital, Baoji, 721008 Shaanxi Province, China

[3]ShengYushou Center of Cell Biology and Immunology, School of Life Sciences and Biotechnology, Shanghai Jiao Tong University, Shanghai 200240, China

[4]Hospital and Institute of Obstetrics and Gynecology, Shanghai Medical College, Fudan University, Shanghai 200032, China

[5]These authors contributed equally

[6]Lead Contact

*Correspondence: qiliang@fudan.edu.cn

https://doi.org/10.1016/j.celrep.2019.02.106

SUMMARY

Aurora kinase B (AURKB), a central regulator of chromosome segregation and cytokinesis, is aberrantly expressed in various cancer cells. However, the relationship of AURKB and oncogenic viruses in cancer progression remains unclear. Here, we reveal that N-cleaved isoforms of AURKB exist in several oncovirus-associated tumor cells and patient cancer tissues, including Kaposi's sarcoma-associated herpesvirus (KSHV), Epstein-Barr virus (EBV), and human papillomavirus virus (HPV). Mechanistically, in KSHV-infected tumor cells, the latent viral antigen LANA cleaves AURKB at Asp^{76} in a serine protease-dependent manner. The N′-AURKB relocalizes to the spindle pole and promotes the metaphase-to-telophase transition in mitotic cells. Introduction of N′-AURKB but not C′-AURKB promotes colony formation and malignant growth of tumor cells *in vitro* and *in vivo* using a murine xenograft model. Altogether, our findings uncover a proteolytic cleavage mechanism by which oncoviruses induce cancer cell segregation and tumorigenesis.

INTRODUCTION

Mitosis is a dynamic and complex process, and the precise control of mitotic regulators is indispensable (Carmena and Earnshaw, 2003; Fu et al., 2007; Gully et al., 2012). Aurora kinase (AURK), a conserved serine and threonine kinase family, plays an essential role in the regulation of the cell cycle and mitosis (Carmena and Earnshaw, 2003; Fu et al., 2007; Gully et al., 2012). Three AURKs have been reported in mammalian cells to date, namely, AURKA, AURKB, and AURKC. AURKC resembles AURKB but regulates both meiosis and mitosis during early development (Carmena et al., 2012). These three members contain a conserved active site within their C terminus, whereas their regulatory domains at the N termini are highly diverse (Brown et al., 2004; Fu et al., 2007). Although the catalytic domains of AURKA and AURKB are highly similar, their biological function and subcellular localization are distinct (Carmena and Earnshaw, 2003). AURKA has been localized to the centrosomes throughout the cell cycle, spreads to the spindle microtubules during metaphase, and relocates to the central spindle in anaphase and telophase, whereas AURKB is mainly located on the centromere in early mitosis, where it serves as a component of the chromosome passenger complex (CPC) and relocates to the midzone or midbody during the cytokinesis. Reports have also revealed that a single amino acid mutant involving G198N converts AURKA into a AURKB-like kinase, which compensates for the loss of AURKB during chromosome misalignment and premature exit of cells from mitosis (Fu et al., 2009). These findings suggest the existence of a compensatory mechanism to rescue the loss of each kinase in mammalian cells.

AURKB is an stringent regulator of chromosome segregation and cytokinesis in mitosis (Terada, 2001). The aberrant expression of AURKB has been detected in various human cancers, leading to chromosomal instability and aneuploidy (González-Loyola et al., 2015; Takeshita et al., 2013). It has been demonstrated that AURKB activity could be regulated in various ways, typically by means of post-translational modifications including phosphorylation (Fu et al., 2007). The spatiotemporal dynamic function of AURKB is mainly due to the stringent control of AURKB protein levels and its kinase activity at different mitotic stages (Gruneberg et al., 2004; Nguyen et al., 2005; Nigg, 2001; Stewart and Fang, 2005; Sugiyama et al., 2002). The autophosphorylation of AURKB at Thr^{232} is essential to AURKB activation (Cheetham et al., 2002; Yasui et al., 2004). The activated AURKB in turn results in the phosphorylation of substrates that are involved in various major mitotic events, including spindle assembly checkpoint, kinetochore attachment, and cytokinesis (Emanuele et al., 2008; Goto et al., 2002; Knowlton et al., 2006). In addition to phosphorylation, other post-translational modifications of AURKB have been shown to regulate its activity and localization. For instance, SUMO modification (SUMOylation) of AURKB at Lys^{207} within the conserved SUMO-modified motif induces the extraction of CPC from chromosomes during prometaphase without affecting its kinase activity (Fernández-Miranda

et al., 2010). However, AURKB modified at Lys^{202} by SUMO-2/3 facilitates AURKB autophosphorylation and activation (Ban et al., 2011), and non-proteolytic ubiquitylation of AURKB by Cul3-based E3 ligases could lead to its displacement from the centromeres to microtubules during mitosis (Krupina et al., 2016; Sumara et al., 2007). In contrast, AURKB degradation depends on proteasomes via the ubiquitin-dependent anaphase-promoting cyclosome complex (APC/c) pathway, which is essential for mitotic exit (Nguyen et al., 2005). Post-translational modification of AURKB predominantly occurs during mitotic regulation, although previous reports have described transcription splicing variants (also known as isoforms) that are potentially correlated with cancer malignancy in hepatocellular carcinoma (Honda et al., 2003; López-Saavedra and Herrera, 2010; Sistayanarain et al., 2006; Yasen et al., 2009). However, understanding of the cause and physical function of these AURKB isoforms is limited.

Cell-cycle manipulation is a common evasion strategy that has been adapted by viruses to achieve a favorable cellular environment for replication and infection (Nascimento et al., 2012; Wei et al., 2016). Kaposi's sarcoma-associated herpesvirus (KSHV), also referred to as human herpesvirus 8 (HHV-8), is well recognized as the causative agent of Kaposi's sarcoma (KS), primary effusion lymphoma (PEL), and multicentric Castleman's disease (MCD) (Davis et al., 2015; Gantt and Casper, 2011). KSHV presents predominantly at the latent stage in most infected host cells. During latency, the KSHV genome persists as a circular episome in the nuclei (Xiao et al., 2010; Ye et al., 2004). To maintain latent infection, it is essential for KSHV to stably sustain its episome in daughter cells during mitosis (Xiao et al., 2010; Ye et al., 2004). LANA, a major latent protein encoded by KSHV, has been shown to play a critical role in tethering KSHV episomes onto the host chromatin by targeting various cellular molecules (Ballestas et al., 1999; Cotter et al., 2001; Jha et al., 2013; Xiao et al., 2010). In contrast, LANA expression, through either KSHV infection or direct transfection, dramatically drives cell growth and enhances chromosome instability (Pan et al., 2004; Si and Robertson, 2006), which is unfavorable for the inheritance of the viral genome during cell division. Thus, it is vital for KSHV to balance viral genome persistence and mediated tumorigenesis by regulating the cell cycle.

In this report, we show that the cleavage of AURKB at the N terminus occurs in the KSHV latently infected tumor cells, which is induced by LANA or KSHV *de novo* infection in a serine protease-dependent manner. Furthermore, the N′-cleaved form of AURKB occurs in other types of malignant tumor cells that are associated with different oncoviruses, including Epstein-Barr virus (EBV) and human papillomavirus virus (HPV). LANA-mediated cleavage of AURKB mainly involves Asp^{76}, and the cleaved large form of $N'_{(77–end)}$ of AURKB relocalizes and promotes the transition from metaphase to telophase during mitosis. The introduction of N′-cleaved instead of C′-AURKB significantly promotes colony formation and malignant growth of tumor cells independent of cell type *in vitro* and *in vivo*. Overall, our findings reveal a proteolytic cleavage of AURKB that generates cleaved forms of AURKB for promoting mitotic progress and tumorigenesis.

RESULTS

Short Forms of AURKB Protein Exist in the Oncovirus-Related Cancer Cells

Previous studies have shown the involvement of AURKA and AURKB in LANA-induced chromosome instability and episome replication during KSHV latency (Cai et al., 2012; Lu et al., 2014). To determine which kinase is mainly associated with LANA, we performed co-immunoprecipitation assays with LANA by overexpressing exogenous AURKA or AURKB with myc tag at its C terminus and LANA in both HEK293T and HeLa cells. AURKA and AURKB did not show any significant difference in the ability to physically interact with LANA. However, a smaller protein band (~35 kDa) of both AURKA and AURKB was consistently and strongly pulled down by LANA (Figure 1A). Because the antibodies against AURKA or AURKB target the myc epitope located at the C terminus of the proteins, the ~35-kDa band may be a short form of the AURKA or AURKB protein, with its N terminus deleted. To confirm the existence of the short form of AURKA or AURKB and their association with LANA, reverse immunoprecipitation using exogenous AURKA or AURKB was conducted, which consistently confirmed that a faster-migrating AURKB protein band with a molecular mass of approximately 35 kDa was induced by LANA, although other short forms were detected (Figure 1B). This implies that LANA not only interacts with AURKB but may also result in the production of small fragments of AURKB via an unknown mechanism.

To determine whether the 35-kDa AURKB occurs at the endogenous level in the KSHV latently infected cells, we first verified two AURKB antibodies that specifically recognize the epitope within the amino acids 1–76 or 250–end region of AURKB, respectively (Figures S1A and S1B). Subsequently, we assessed the protein profiles of endogenous AURKB expression in both the KSHV-negative cell line (BJAB) and the KSHV-positive cell lines (BCBL1, BC3, and JSC1) using the two AURKB antibodies. Figure 1C shows that a N′-short band of AURKB with a molecular mass of approximately 35 kDa was detected in all KSHV-positive cell lines using the AURKB(C) antibody targeting the C terminus of AURKB but was rarely detected in KSHV-negative cell lines, although a relatively weaker C′-short band with a molecular mass of approximately 40 kDa (larger than the N′-short band of 35 kDa) was also observed using the AURKB(N) antibody that targeted the N terminus AURKB. In contrast, the N′-short band (~35 kDa) was not detected in the immunoblotting assay with the AURKB(N) antibody, indicating that the N′-short band is the product of AURKB after deletion of the N terminus. The human umbilical vein endothelial cells (HUVECs) subjected to KSHV *de novo* infection *in vitro* showed a 2- to 6-fold increase in the level of the N′-short form (instead of the C′-short form) of the AURKB protein two to five days post-infection (Figure 1D). To explore whether these N′-short forms of AURKB are also induced by other types of oncoviruses, including EBV and HPV, we examined these oncovirus-related cancer cells with or without viral infection. We observed a similar phenomenon of increased levels of the N′-short form of the AURKB protein in cells upon infection with EBV, or HPV (Figures 1E and 1F). Three transcriptional splicing variants of AURKB in hepatocellular carcinoma

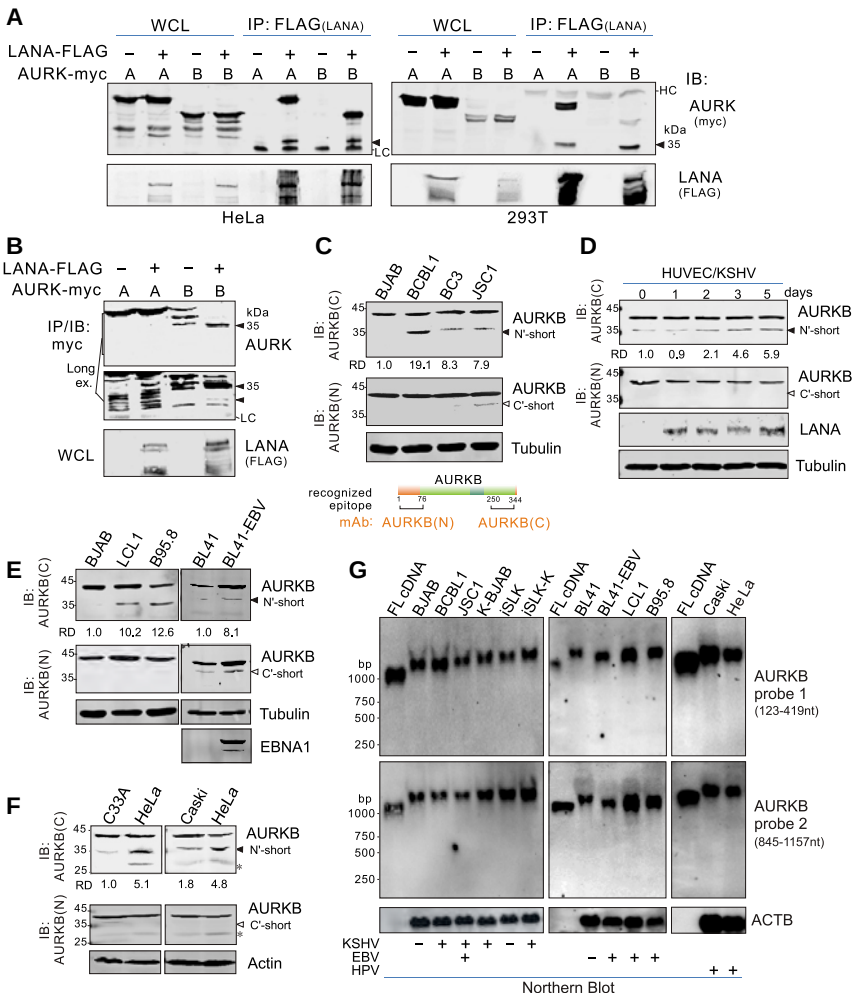

Figure 1. Short Forms of AURKB Protein Exist in the Oncovirus-Associated Cancer Cells

(A) LANA interacts with short forms of exogenous AURKA or AURKB. HeLa and HEK293T cells were individually transfected with expression plasmids as indicated. At 48 h post-transfection, 15 × 10^6 cell lysates were subjected to immunoprecipitation (IP) and immunoblotting (IB) as indicated in the figure. WCL, whole-cell lysate; HC, heavy chain; LC, light chain. The arrow shows the short form (~35 kDa) of AURKA or AURKB pulled down by LANA.

(B) Short form of AURKA or AURKB is induced by LANA. HEK293T cells were individually transfected with expression plasmids as indicated. At 48 h post-transfection, 15 × 10^6 cell lysates were subjected to immunoprecipitation (IP) and immunoblotting (IB) as indicated in the figure.

(C) Short form of endogenous AURKB highly exists in PEL cells. Cell lysates from equal amounts of KSHV-infected PEL (BCBL1, BC3, and JSC1) cells and uninfected BJAB cells were subjected to immunoblotting (IB) analysis with antibodies as indicated in the figure. Molecular weight markers in kilodaltons (kDa) are indicated to the left of the blot.

(D–F) Short form of endogenous AURKB is increased in (D) HUVECs with KSHV *de novo* infection, (E) EBV-uninfected (BJAB and BL41) and EBV-infected (LCL, B95.8, and BL41-EBV) lymphoma cells, and (F) HPV-uninfected (C33A) and HPV-infected (Caski and HeLa) cervical cells.

(G) Northern blot analysis of mRNA transcripts of endogenous AURKB in the KSHV-, EBV-, or HPV-infected and uninfected cells. Total RNA extracted from each cell line was subjected to northern blot assays with AURKB probes as indicated. β-actin (ACTB) was used as internal control. Relative density (RD) of the N′-short form of AURKB is quantified. An asterisk indicates uncharacterized bands. Bottom: status of viral infection in each cell line is indicated.

(HCC) have been previously reported (Honda et al., 2003; López-Saavedra and Herrera, 2010; Sistayanarain et al., 2006; Yasen et al., 2009). To exclude the possibility that the N′-short form of AURKB induced by oncovirus infection is due to splicing variants of AURKB at the transcription level, we examined the transcripts of both endogenous and exogenous AURKB upon KSHV infection (or expression of its latent antigen LANA) by conducting northern blot and RT-PCR assays, respectively. The northern blot results showed that no additional faster-migrating AURKB mRNA transcripts in the KSHV-infected cells were detected using either N (123–419 nt)-terminal or C (845–1,157 nt)-terminal targeted probes (Figure 1G, left; Figure S2A), and no additional splicing variants of endogenous AURKB appeared in the KSHV-infected cells or exogenous AURKB in the presence of LANA using RT-PCR with specific primer set, respectively (Figures S2B and S2C). Similar results from cells infected with EBV or HPV were observed (Figure 1G, right), confirming that the appearance of the N′-short form of the AURKB protein was generated in response to oncovirus infection by directly or indirectly cleaving AURKB.

To confirm that this N′-short form of AURKB occurs in virally infected primary cancer tissues, we collected the KSHV-, and HPV-related patient cancer tissues and performed similar immunoblotting assays. In the KSHV-associated KS tissues, the enhanced N′-short form of the AURKB protein occurred compared to the KSHV-free oral skin lesion tissues, although a smaller band (~25 kDa) appeared in addition to the molecular mass protein band of 35 kDa (Figure 2A). These findings suggest that the short forms of AURKB are related to KSHV infection. For the cervical cancer tissues with or without HPV infection, we collected cervical tissues from patients diagnosed with HR-HPV but negative for intraepithelial lesion or malignancy (NILM, HPV−), atypical squamous cells of undetermined significance (ASC-US, HPV+), and squamous cell carcinoma (SCC, HPV+). The results of the immunoblotting assays using AURKB antibodies consistently showed that the N′-short form instead of the C′-short form of AURKB predominated in all SCC tissues (10 of 10 versus 4 of 10 cases), whereas AURKB was barely detectable in either NILM or ASC-US. The major molecular weight of the AURKB N′-short form in SSC tissues is also ~35 kDa, although weaker bands were detected (Figures 2B and 2C). The abundance of the N′-short form of AURKB in SCC tissues is strongly associated with metastatic cervical cancer (4 of 10 cases).

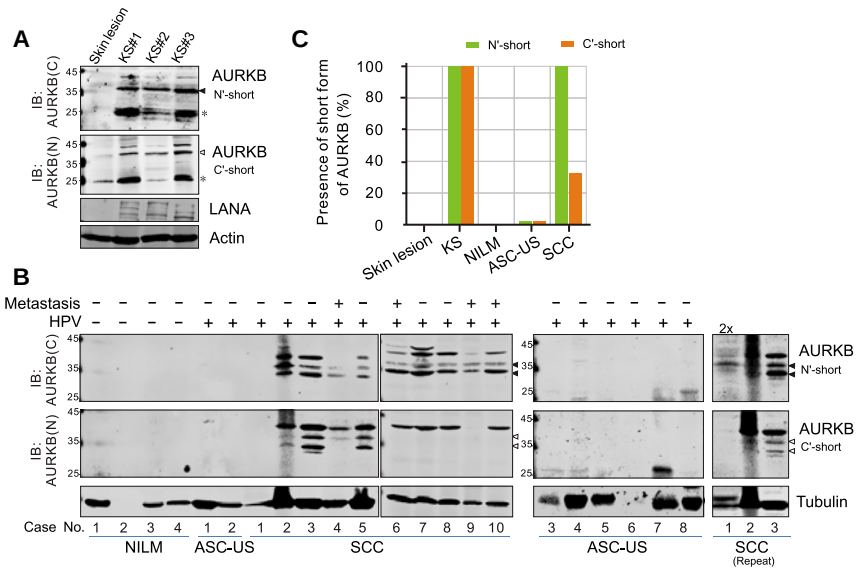

Figure 2. Short Forms of Endogenous AURKB Are Highly Presented in the Oncovirus-Associated Cancer Tissues

(A and B) KSHV-infected Kaposi's sarcoma (KS) (A) and HPV-infected cervical squamous cell carcinoma (SCC) (B). Cell lysates from equal amounts of patient tissues were subjected to immunoblotting (IB) analysis with antibodies as indicated in the figure. A KSHV-free oral skin lesion tissue is used as the control. An asterisk indicates uncharacterized bands. Top: metastasis and HPV infection in cervical tissues are shown.

(C) Percentage of the presence of short forms of AURKB in each type of tumor cell was calculated from (A) and (B). The potential cleavage product of the amino (N′) or C′ terminus is indicated by triangles.

The Oncovirus KSHV Induces N Cleavage of AURKB on Asp^{76}

To elucidate the cleavage site in AURKA and AURKB, we first analyzed the similarity in the functional domains in both AURKA and AURKB and hypothesized that the cleavage sites of both proteins are situated within conserved sequences of the activation domains based on the production of similar-molecular weight (~35 kDa) N′-short forms (Figures 1A and 1B). To test this, we generated AURKA or AURKB with a GFP tag at the N terminus and co-expressed this with or without LANA in HEK293T cells, followed by immunoblotting with GFP antibody. Figures 3A and 3B show a fast-migrating band with a molecular mass of approximately 36 or 33 kDa (the size represents the protein containing GFP and the N fragment cleaved from AURKA and AURKB, respectively) on LANA co-transfected with the GFP-AURKA or GFP-AURKB samples. In contrast, we observed a smaller-molecular weight protein band of approximately 25 kDa exclusively in AURKB with LANA co-expression (Figure 3B, compare lanes 2 and 6 with lanes 1 and 5). Considering that AURKB plays critical roles in mitosis through its kinase activity (Honda et al., 2003), the kinase-inactive mutants K162R in AURKA and K106R in AURKB were found to prevent the protein cleavage fate mediated by LANA (Figure 3B, compare lanes 2 and 6 with 2 and 8), which indicates that LANA-induced cleavage of AURKA and AURKB mainly occurs in a mitotic progress and depends on kinase activity.

To confirm that AURKB is susceptible to cleavage by LANA at its N-terminal region, a series of N- and C-terminal truncated mutants of AURKB with a GFP tag were generated (Figure S3A). The results of the immunoblotting assays using the GFP antibody on HEK293T cells co-expressing these truncated mutants with or without LANA showed that except for full-length AURKB and the truncated mutant 1–195 aa, both N and C terminus truncated mutants of AURKB did not clearly exhibit cleavage in the presence of LANA compared to the absence of LANA (Figure S3B). Further experiments from co-immunoprecipitation assay showed that LANA bound to the C terminus (250–344 aa) instead of the N terminus (1–76 aa) of AURKB (Figure S3C). This indicates that the LANA-mediated cleavage site of AURKB is located within its N terminus, which requires the presence of the C termini of AURKB. However, the cleavage of mutant 1–195 aa induced by LANA could be caused by the second effect due to the loss of residue 195–250 aa (which contains an activation loop) of AURKB.

To further investigate the potential cleavage sites within the N terminus of AURKB, we analyzed the whole amino acid sequences of AURKB, along with AURKA, for peptidase-mediated cleavage sites using MEROPS database online prediction software (Rawlings et al., 2018). Coinciding with our previous observations, two potential cleavage sites within the homologous region of both AURKB and AURKA have been previously shown by mass spectroscopy analysis (Schilling and Overall, 2008), as well as the additional site Met^{1} (M1) in AURKB (Figure 3A). In addition, the two sites Asp^{76} (D76, which is Asp^{132} [D132] in AURKA) and Lys^{85} (K85, which is Lys^{141} [K141] in AURKA) are predicted to be cleaved by peptidase HIV retropepsin and trypsin, respectively (Figure 3A), whereas M1 is targeted by an unknown peptidase. Surprisingly, CaspDB database online analysis (Kumar et al., 2014) indicated that the D75 position in AURKB has a high probability score (>0.7) for caspase-mediated cleavage, and four additional potential cleavage sites, namely, D186, D238, D255, and D255, within the C termini of AURKB with high scores (>0.6) were identified. However, we did not observe the corresponding cleavage of AURKB at its C terminus by LANA in the previous immunoblotting assays (Figure 3B, lanes 5 and 6). Based on these prediction results, the GFP-tagged AURKB mutants containing the single mutations of K85A, D76A, and D76R or double mutation of D76,85A were individually generated (Figure 3C) and overexpressed in HEK293T cells with or without LANA, followed by immunoblotting with GFP antibody as previously described. The LANA-mediated cleavage in both D76 and M1 residues was significantly reduced in AURKB bearing the D76 mutation (D76A, D76R, and D76,85A), although AURKB with the K85A mutation showed an apparent increase in cleavage sensitivity at D76 (Figure 3B, lanes 9–16).

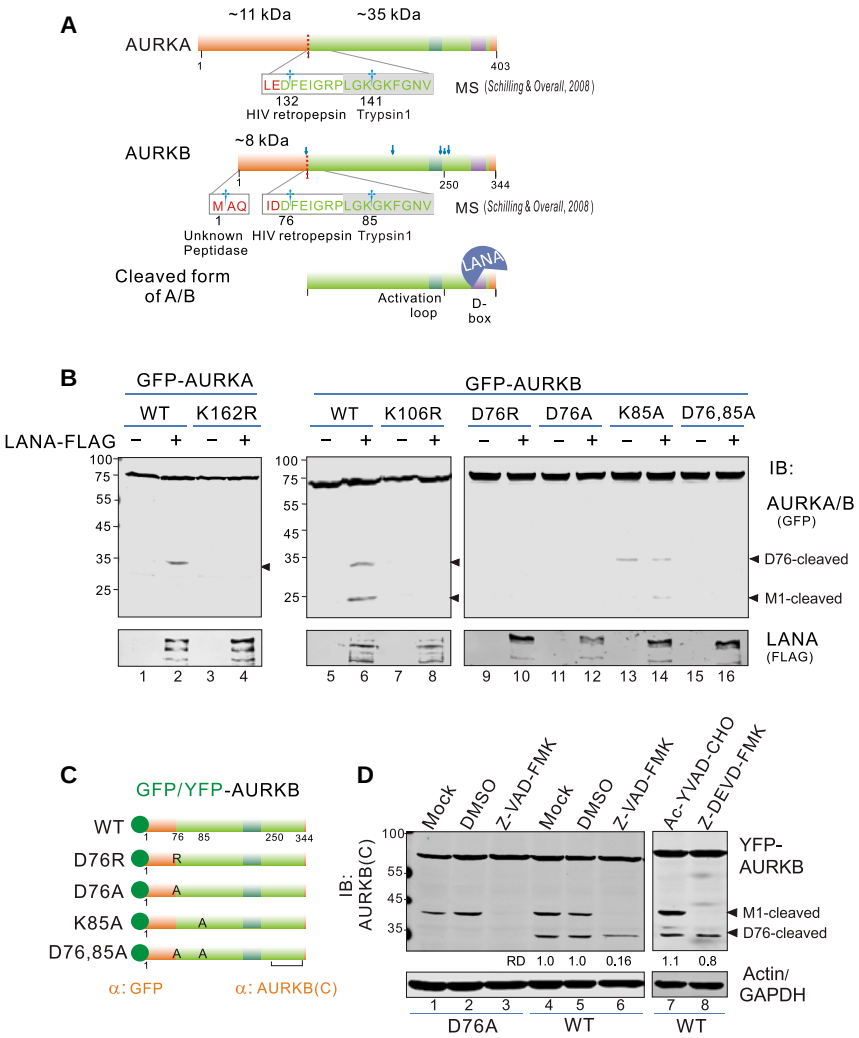

Figure 3. Oncovirus KSHV Induces AURKB Cleavage on Asp[76]

(A) Schematic of cleaved sites of AURKA or AURKB predicted by online database analysis. A star indicates the potential cleaved sites from analysis of the MEROPS database in mass spectroscopy (Schilling and Overall, 2008). An arrow indicates the potential cleaved sites from analysis of the CaspDB database. The regulatory domain (orange), catalytic domain (green), activation loop (dark green), nucleotide binding domain (gray), and D-box domain (purple) of AURKB that bind to LANA are indicated in rectangles.

(B) LANA-induced AURKB cleavage on Asp[76] residue is impaired by mutation of the kinase activation site. HEK293T cells were transfected with expression plasmids as indicated. At 48 h post-transfection, cells were subjected to immunoblotting (IB) with antibodies against the indicated proteins. Molecular weight markers in kilodaltons (kDa) are indicated to the left of the blot.

(C) Schematic of wild-type AURKA or AURKB and its site mutants with a GFP or YFP tag. The position of the epitope recognized by antibodies against GFP and AURKB(C) in the GFP/YFP-tagged AURKB protein is shown.

(D) Inhibitor of pan caspase, but not caspase-1 and caspase-3 and -7, blocks exogenous AURKB cleavage at Asp[76]. Equal amounts of KMM-stable cells with YFP-tagged wild-type (WT) AURKB or D76A mutant expression were individually untreated (mock) and treated with inhibitors of pan caspase (Z-VAD-FMK, 25 μM), caspase-1 (Ac-YVAD-CHO, 25 μM), and caspase-3 and -7 (Z-DEVD-FMK, 25 μM) or DMSO for 24 h, followed by immunoblotting analysis with antibodies as indicated. The M1- and D76-cleaved forms of AURKB are indicated by arrows. Relative density (RD) of the D76-cleaved band is quantified and shown.

To confirm the preceding observation in a physiological condition, we used KSHV-transformed rat embryonic metanephric mesenchymal precursor (KMM) cell lines (a primary rat embryonic metanephric mesenchymal precursor cell with KSHV latent infection) to stably express yellow fluorescent protein (YFP)-tagged wild-type AURKB or its D76A mutant using a lentivirus system, followed by immunoblotting as previously described. By using the AURKB(C) antibody that only recognizes human AURKB instead of rat, we found that in these two YFP-AURKB-stable expression cell lines, the D76A mutation effectively blocks the cleavage of AURKB at D76 and moderately reduces the cleavage at M1 compared to wild-type AURKB (Figure 3D, lanes 1 and 4). To further determine the potential cleavage effect of caspase activity on D76 residue, we treated these two stable cell lines with different caspase inhibitors or DMSO as the control. The results of immunoblotting showed that treatment with Z-VAD-FMK (an inhibitor of pan caspases) instead of Ac-YVAD-CHO (an inhibitor of caspase-1) or Z-DEVD-FMK (an inhibitor of caspase-3 and -7) could efficiently block the cleavage of AURKB at D76 (Figure 3D, compare lanes 5 and 6 with lanes 7 and 8). In addition, we observed that cleavage of AURKB at M1 in both wild-type AURKB and its D76A mutant is abolished by both Z-VAD-FMK and Ac-YVAD-CHO, but not Z-DEVD-FMK (Figure 3D, lanes 3, 6, and 8). These findings confirm the conclusion that the N′-cleavage site of AURKB induced by LANA mainly occurs at D76.

KSHV-Induced Cleavage of AURKB Relies on a Serine Protease

We showed earlier that the cleavage sites D76 and K85 of AURKB identified by the MEROPS database are predicted to be sensitive to peptidase HIV retropepsin (an aspartyl protease) and trypsin (a serine protease), respectively. To identify the type of protease that plays a key role in LANA-induced cleavage of AURKB, we treated cells with inhibitors of aspartyl protease (pepstatin) or serine protease (phenylmethanesulfonyl fluoride [PMSF] or aprotinin). The HEK293T cells transiently co-expressing myc-tagged AURKB with or without FLAG-tagged LANA, followed by treatment with different protease inhibitors for 6 h showed that the cleaved AURKB products induced by LANA are significantly inhibited by either PMSF or aprotinin compared to the control group (Figure S4). In contrast, treatment with pepstatin did

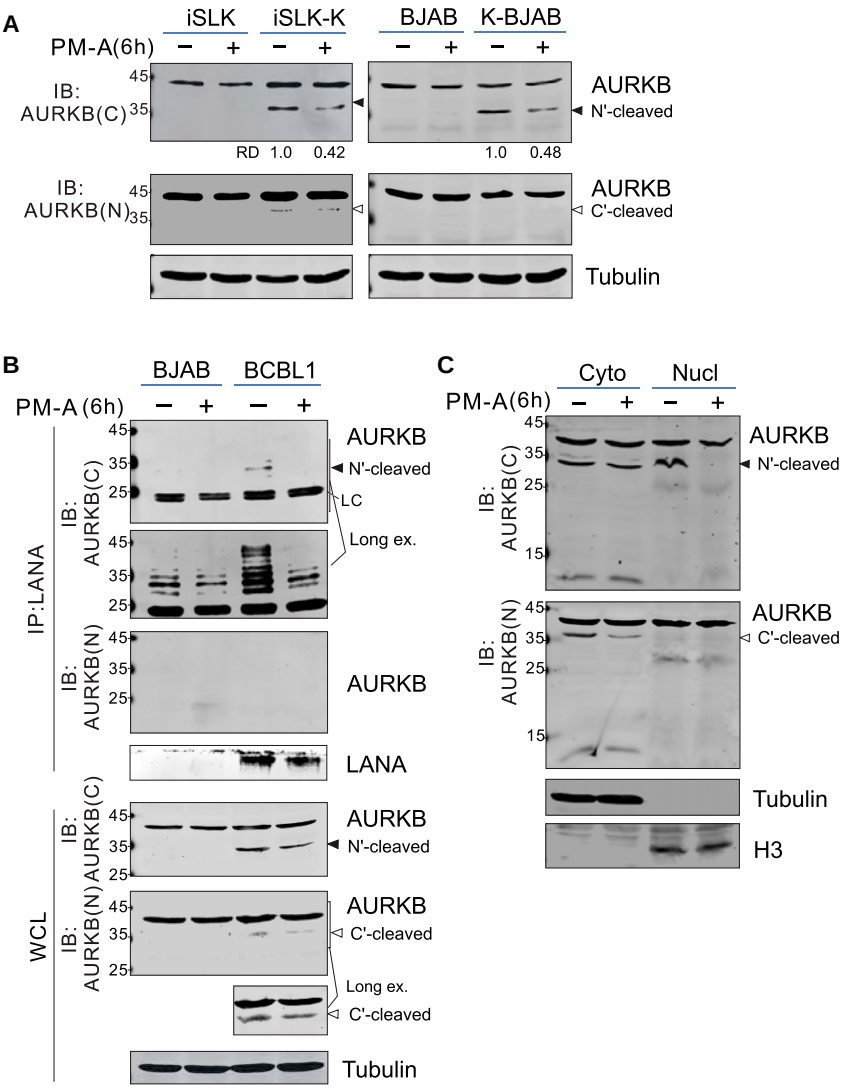

Figure 4. Cleavage of Endogenous AURKB Occurs in KSHV Latently Infected Cells and Is Blocked by Serine Protease Inhibitors

(A) Serine protease inhibitors block cleavage of endogenous AURKB. 20 × 10^6 cell lysates from equal amounts of KSHV-infected and uninfected cells treated with or without serine protease inhibitors PMSF and aprotinin (PM-A) for 6 h were subjected to immunoblotting (IB) analysis with antibodies as indicated in the figure. Tubulin was used as internal control.

(B) N-cleaved form of AURKB is highly associated with LANA in PEL cells. Cell lysate from BCBL1 and BJAB cells treated as in (A) were subjected to co-immunoprecipitation (coIP) with LANA, followed by immunoblotting (IB) analysis with antibodies as indicated in the figure.

(C) Serine protease inhibitors block N cleavage of AURKB in nucleus. Immunoblotting (IB) analyses of fractionated proteins from iSLK-K cells with or without serine protease inhibitors treatment for 6 h. WCL, whole-cell lysate. Arrow shows the N- and C-cleaved AURKB proteins.

not disrupt AURKB cleavage by LANA. To define whether cleavage of endogenous AURKB is also sensitive to the serine protease inhibitor, KSHV-infected and uninfected cells were subjected to treatment with either PMSF-aprotinin or DMSO control for 6 h, followed by immunoblotting with AURKB(N) and AURKB(C) antibodies. In the presence of PMSF-aprotinin, a more than 2-fold decrease in the amount of N′-AURKB at D76 was observed in both BJAB and iSLK cells induced by KSHV infection, as well as in BCBL1 cells, whereas no major change in the amount of C′-AURKB was observed (Figures 4A and 4B), supporting our hypothesis that KSHV-induced N′ cleavage of AURKB is mediated by serine proteases. In addition, we observed that LANA preferentially binds to the $N'_{(77–end)}$-cleaved form of endogenous AURKB with the C terminus than the intact AURKB in BCBL1 cells, which is significantly inhibited by treatment with PMSF-aprotinin (Figure 4B, top). The results of cell compartment fraction assays revealed that the $N'_{(77–end)}$-cleaved form of AURKB is almost equally distributed in both the cytoplasm and the nucleus, whereas nuclear localization is significantly blocked by PMSF-aprotinin (Figure 4C). In contrast, the C′-cleaved form of AURKB was exclusively located in the cytoplasm and was partially impaired by PMSF-aprotinin (Figure 4C). This indicates that the nuclear localization of the $N'_{(77–end)}$-cleaved form of AURKB facilitates its interaction with LANA within the nucleus.

The $N'_{(77–end)}$-AURKB by LANA Precisely Controls the Transition between Mitotic Phases

LANA is a major contributor to the faithful segregation of the viral genome into daughter cells during mitosis (Ye et al., 2004). Nguyen and colleagues previously showed that AURKB protein levels and kinase activity are tightly controlled to ensure accurate transitions between phases of mitosis (Nguyen et al., 2005). Given our previous observations that the kinase-inactive K106R mutant abolishes LANA-mediated cleavage of AURKB, we hypothesized that the cleavage of AURKB could be an alternative strategy used by LANA to modulate mitotic progress. To test this hypothesis, we assessed the distribution of different phases of the cell cycle and the level of multinuclear cells in HEK293T cells overexpressing GFP-tagged wild-type AURKB or its kinase-inactive mutant K106R in the presence or absence of red fluorescent protein (RFP)-tagged LANA by cell-imaging flow cytometry. The results showed that the overexpression of wild-type AURKB, but not its kinase-inactive K to R mutation, enhances the percentage of cells at the G2/M phase, which is abolished by co-expression with LANA (Figure S5A, right). However, further investigation of the distribution ratio of cells with different mitotic phases (particularly prophase, metaphase, anaphase, and telophase) in the G2/M populations of AURKB-overexpressing cells did not show significant difference between

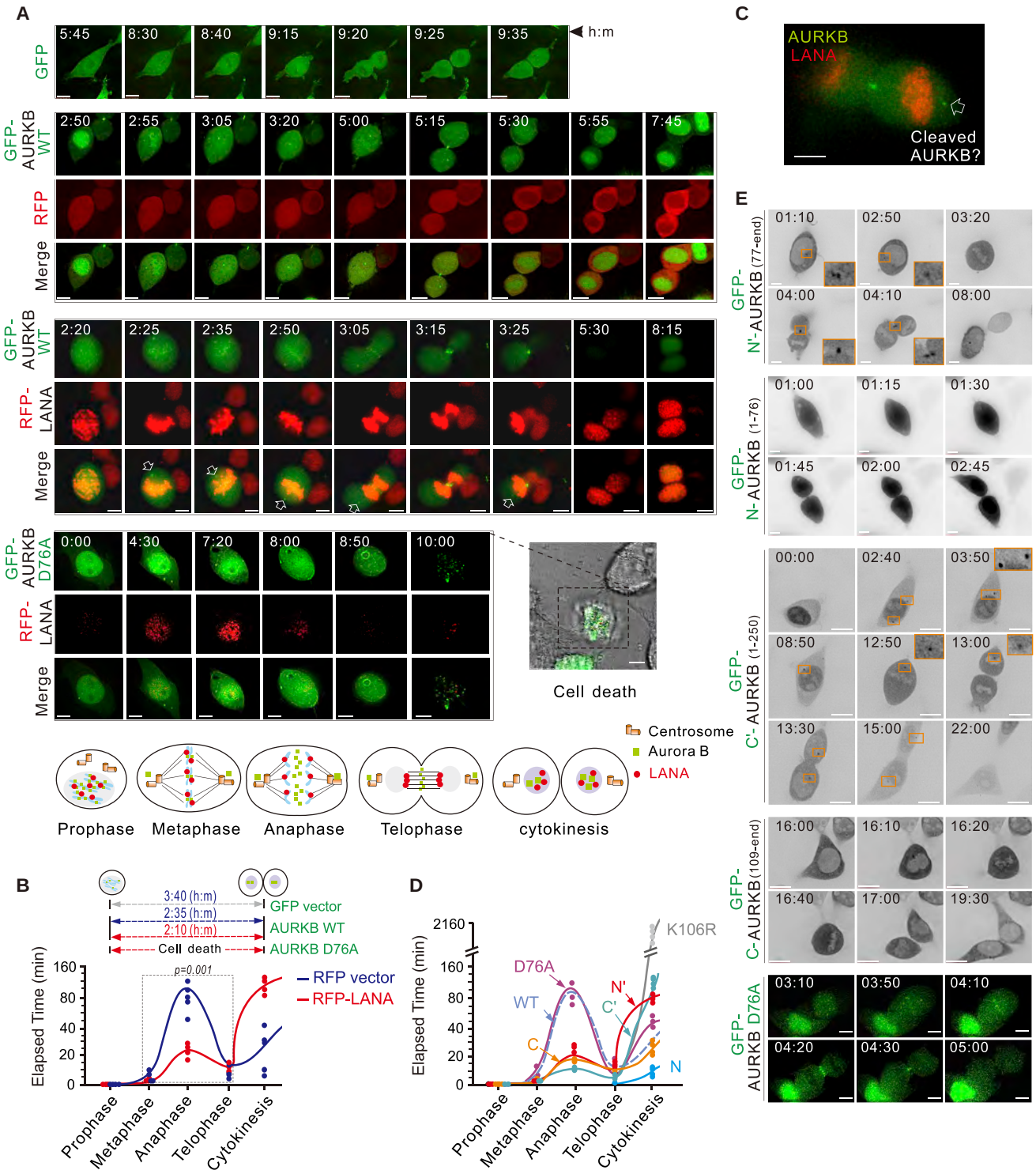

Figure 5. LANA-Mediated Cleavage of AURKB Enhances Mitotic Cell Segregation

(A) HEK293T cells were transiently transfected with the combined expression plasmids as indicated. 24 h post-transfection, living cells were monitored by time-lapse fluorescence microscopy (scale bar, 5 μm). Bottom: schematic of localizations of GFP-AURKB in mitotic cells with RFP-LANA co-expression is shown.

(B) Quantitative characterization of duration of mitotic cells from prophase to cytokinesis in (A). Cells were classified by chromosome and cell morphology. Each data point represents three independent experiments, each measuring 10 mitotic cells.

(C) Representative mitotic cells at telophase with GFP-AURKB and RFP-LANA co-expression in (A) (scale bar, 5 μm). The localization of AURKB at polar of centrosome is indicated by an arrow.

(legend continued on next page)

the presence and the absence of LANA (Figure S5A, middle). Overexpression of AURKA and its K to R mutation in an identical experiment revealed a similar phenomenon (Figure S5A, bottom). Only AURKA instead of AURKB co-expression with LANA resulted in an increase in the percentage of multinuclear cells (2N and 3N), which agrees with the findings of a previous study (Cai et al., 2012). This finding indicates that cleavage of AURKB may contribute to the cellular exit from the G2/M phase, which depends on kinase activity.

To confirm whether LANA-mediated AURKB cleavage affects the elapsed time of the mitotic cell progress, HEK293T cells transiently co-transfected GFP-AURKB or GFP-AURKB-D76A with RFP-LANA or vector alone were assessed to determine the time of transition between stages of mitosis using live-cell imaging. The results showed that LANA effectively reduces the average transition time from prophase to telophase in cells expressing GFP-AURKB compared to GFP-AURKB alone (Figures 5A and 5B). The average time from telophase to cytokinesis was extended in the presence of LANA, which in turn moderately shortened the overall time of mitosis from prophase to cytokinesis in cells co-expressing exogenous AURKB and LANA compared to cells expressing exogenous AURKB alone (Figure 5B). In contrast, a high proportion (5 of 6) of cells co-expressing GFP-AURKB-D76A and LANA had difficulty entering or completing mitotic progress, and cells died during the 24-h monitory period, which indicates a critical role of the AURKB cleavage at D76 in LANA-mediated cell mitosis (Figures 5A and 5B). In addition, we observed distinct punctate signals of exogenous AURKB distributed in the poles of cells co-expressing LANA during mitosis, which is distinct from the typical distribution of AURKB (Figure 5C). These results suggest that LANA plays a fine-tuning regulatory role in mitotic progress by targeting AURKB cleavage and that elongation of the transition between telophase and cytokinesis in mitosis presumably facilitates in the efficient and faithful inheritance of the viral episome.

Next, the dynamic transition time between mitotic phases was monitored by live-cell imaging of HEK293T cells transiently expressing different cleaved forms of GFP-tagged AURKB mutants, including $N'_{(77–end)}$-AURKB, $N_{(1–76)}$-AURKB, $C'_{(1–250)}$-cleaved AURKB, and $C_{(109–end)}$-AURKB, along with wild-type AURKB and its kinase-inactive K106R mutant. Figures 5D and 5E show that the expression of the cleaved forms of AURKB significantly reduced the average time from prophase to telophase compared to wild-type AURKB, which agrees with the phenomenon of cells co-expressing GFP-AURKB with LANA (Figure 5B), although the dominant-negative K106R mutation results in the disruption of cell division (Figure S5B) (King et al., 1996). The expression of $N_{(1–76)}$-AURKB in HEK293T cells shortened the transition time from telophase to cytokinesis, whereas the effect in HEK293T cells expressing $N'_{(77–end)}$-AURKB or $C'_{(1–250)}$-cleaved AURKB was similar to that in the presence of LANA, which involved an increase in the time required from telophase to cytokinesis relative to the wild-type AURKB (Figure 5D). Both large cleaved forms of AURKB, $N'_{(77–end)}$-AURKB and $C'_{(1–250)}$-cleaved AURKB mutants, appeared as punctate signals during mitosis, although the punctate dots of $N'_{(77–end)}$-AURKB were mainly located at the midbody during cytokinesis, and $C'_{(1–250)}$-cleaved AURKB is located at the poles of mitotic cells (Figure 5E), which is similar to that in cells co-expressing exogenous GFP-AURKB with LANA. In contrast, the two termini-cleaved forms of $N_{(1–76)}$-AURKB and $C_{(109–end)}$-AURKB were distributed in whole cells and cytoplasm during mitosis, respectively (Figure 5E). The D76A mutant presents an effect similar to that of wild-type AURKB in mitotic progress but prolongs the transition time from telophase to cytokinesis (Figures 5D and 5E). These findings confirm that LANA-mediated cleavage of AURKB involves the modulation of mitotic progress, particularly the transition from telophase to cytokinesis.

Cleaved AURKB Cooperates with AURKA during Mitosis

Because both AURKA and AURKB share highly functional similarities (Carmena and Earnshaw, 2003; Fu et al., 2009) and the punctate signals of $C'_{(1–250)}$-cleaved AURKB are located at the poles of mitotic cells, we hypothesized that the $C'_{(1–250)}$-cleaved AURKB has an AURKA-like function during mitosis. To test this hypothesis, HEK293T cells co-expressing exogenous GFP-tagged wild-type (WT) AURKB, $N'_{(77–end)}$-AURKB, or $C'_{(1–250)}$-cleaved AURKB with mCherry-tagged AURKA were monitored by time-lapse cell-imaging microscopy. The results showed that the punctate signals of $C'_{(1–250)}$-cleaved AURKB instead of $N'_{(77–end)}$-AURKB completely co-localized with AURKA at the spindle pole of mitotic cells, particularly during the transition from metaphase to cytokinesis (Figure 6A). In contrast, the punctate signals were rarely observed in the group of exogenous AURKB-WT and AURKA co-expression. Unexpectedly, co-expression of WT AURKB or its mutants ($N'_{(77–end)}$-AURKB and $C'_{(1–250)}$-cleaved AURKB) exclusively extended the time required from metaphase to cytokinesis in AURKA-expressing cells compared to AURKA alone (Figure 6A). This finding suggests that both cleaved forms of AURKB, N′ cleaved and C′ cleaved, coordinate with AURKA in driving mitotic cell progression, although the punctate signals of N′-AURKB distinct from C′-AURKB did not completely co-localize with AURKA at the spindle poles.

To determine whether the spindle pole localization of endogenous AURKB exists, BCBL1 cells were assessed by immunofluorescence confocal microscopy using AURKB(N)- and AURKB(C)-specific antibodies targeting the N termini and C termini, respectively. Consistent with previous observations,

(D) Quantitative characterization of the elapsed time from prophase to cytokinesis of mitotic cells expressing different AURKB mutants. HEK293T cells were individually transfected with K106R (Figure S5B), D76A, N terminus (N, 1–76 aa), N-cleaved (N′, 77–end aa), C terminus (C, 109–end aa), and C-cleaved (C′, 1–250 aa) mutants of AURKB with a GFP tag. 24 h post-transfection, live cells were monitored by time course fluorescence microscopy. Cells were classified by chromosome and cell morphology. Each data point represents 3 independent experiments, each measuring 10 mitotic cells. WT AURKB from (B) is included and shown as a dash line.

(E) Representative images of living cells expressing different GFP-tagged AURKB mutants with distinct localization patterns were performed as in (A) (scale bar, 5 μm). Punctate dots of N′-AURKB and C′-AURKB mutants in different phases of the cell cycle are indicated by boxes.

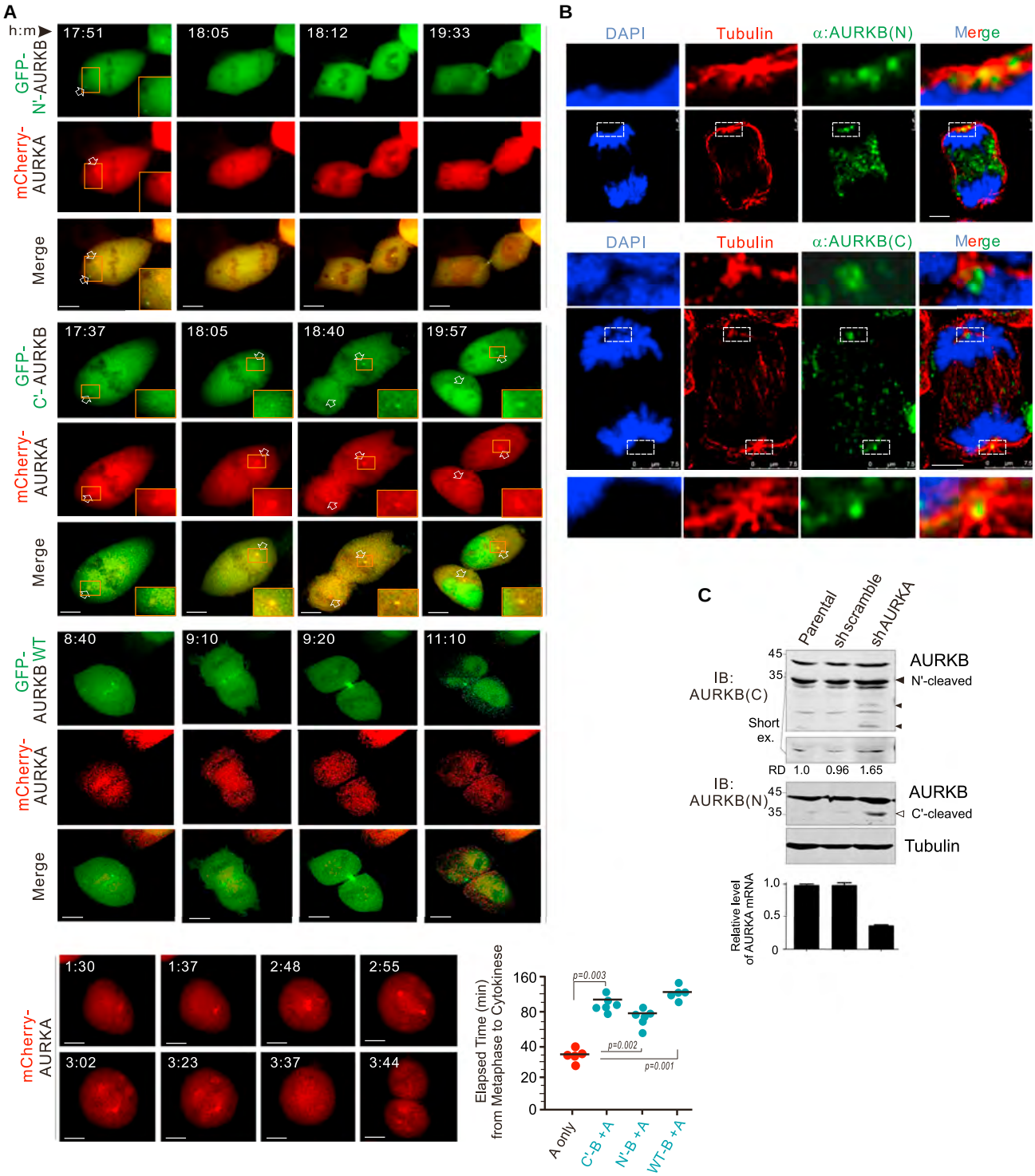

Figure 6. Cleaved Form of AURKB Cooperates with AURKA in Mitosis

(A) C-cleaved form instead of N-cleaved form of AURKB co-localizes with AURKA at the centrosome in mitosis (scale bar, 5 μm). HEK293T cells were individually transfected with mCherry-tagged AURKA in the presence of GFP-tagged N′-AURKB (N-cleaved) mutant, C′-AURKB (C-cleaved) mutant, or alone. 24 h post-transfection, living cells were monitored by time-lapse fluorescence microscopy. Representative images of living cells expressing different AURKB and AURKA mutants are shown. Punctate dots of N′-AURKB and C′-AURKB mutants and AURKA in different mitotic phases are indicated by boxes and arrows. Bottom: quantitative analysis of elapsed time from metaphase to cytokinesis of transfected cells is shown (means ± SEM, n = 6, t test). $p < 0.05$, significant; $p > 0.05$, non-significant.

(legend continued on next page)

the results showed that a portion of endogenous AURKB in two cases localized at the region of the spindle pole, which is distinct from the typical localization of full-length AURKB in mitosis (Figure 6B; Video S1). This indicates the untypical pole localization of AURKB most likely results from the N′-cleaved and C′-AURKB. Knocking down endogenous AURKA resulted in higher amounts of C′-AURKB in BCBL1 cells, whereas the level of N′-AURKB is not evident in the molecular weight of 35 kDa but is clearer in the smaller-molecular weight protein bands (Figure 6C), supporting the notion that the cleaved AURKB compensates for AURKA during mitosis.

N′-AURKB Promotes KSHV-Infected Tumor Cell Growth and Malignancy

To elucidate the physiological function of AURKB cleavage in KSHV-infected cells, equal amounts of iSLK cells and their derivative KSHV-infected iSLK-K cells were individually treated with the inhibitor of AURKB cleavage or mock control and assessed using a colony formation assay. The results of a 12-day culture showed a reduction in colony formation in iSLK-K cells treated with the protease inhibitor PM-A, but not in iSLK cells compared to control (Figure 7A, left). A similar inhibitory effect was observed in KSHV-infected KMM endothelial cells (Figure 7A, right). In addition, significant inhibition of the proliferation of PEL, BCBL1, and KSHV-infected BJAB cells was observed after treatment with PM-A, whereas that of BJAB cells were not significantly affected (Figure S6A). To confirm the role of cleaved AURKB in the growth of KSHV-infected cells, we generated KMM and BCBL1 cells (which represent two main types of cells infected by KSHV, namely, endothelial and B cells) stably expressing $N'_{(77–end)}$-cleaved, $C'_{(1–250)}$-cleaved AURKB, or D76A mutants, along with WT AURKB and vector as controls (Figure S6B). Similarly, the results of cell colony formation assays showed that N′-AURKB enhances colony formation in both KMM and BCBL1 cells *in vitro* when compared to the vector alone, whereas WT AURKB showed a dramatic reduction (Figure 7B; Figure S6C). In contrast, the C′-AURKB and D76A mutant presented opposite effects in two types of cells (Figure 7B; Figure S6C). The results of cell-cycle analysis revealed that distinct from WT AURKB that promotes cell transition from S to G2/M phase, both N′-AURKB and C′-AURKB do not significantly alter the cell cycle compared to the vector alone (Figure 7C; Figure S6D). Unexpectedly, the D76A mutant caused a ~3.9- and ~3.2-fold increase in cell apoptosis (subG1 population) in both KMM and BCBL1 cells, respectively, although it presented the opposite effect in colony formation and transition from S to G2/M phase in these two cell lines, indicating that the inhibition of AURKB cleavage at D76 induces cellular apoptosis. In the tumor xenograft model of PEL cells *in vivo*, N′-AURKB instead of C′-cleaved or WT AURKB consistently caused higher tumor growth rates (126-fold versus 67.9-fold) within five weeks after injection and malignancy (~55% versus 100% survival at 90-day post-injection) compared to vector-alone control (Figure 7D, bottom), although the D76A mutant also increases tumor growth (107-fold versus 67.9-fold) and malignancy (~78% versus 100% survival) to some extent. Thus, these findings support our hypothesis that N′ cleavage of AURKB at D76 promotes KSHV-infected tumor cell growth and malignancy.

DISCUSSION

We and other colleagues have previously reported that serine/threonine protein kinase AURKA or AURKB plays a role in KSHV-induced chromosome instability and host cell survival (Cai et al., 2012; Lu et al., 2014). Because AURKB is known as an aberrantly expressed gene in many cancer and tumor cell lines and regulates accurate chromosomal segregation, cytokinesis, and mitotic checkpoint (Giet et al., 2005), we are interested in understanding how AURKB is modulated by KSHV for cell segregation during latency. Although AURKB has been reported to be associated with LANA in the activation of phosphorylation of survivin and increasing viral genome replication (Lu et al., 2014), the molecular mechanism and the biological effects of AURKB in KSHV-induced cell segregation and tumorigenesis remain unclear. Here, we propose that the cleavage of AURKB at the N terminus is highly induced by KSHV during latent infection and drives cell segregation and tumorigenesis, which is achieved by the latent antigen LANA in a serine protease-dependent manner. More importantly, we observed that similar proteolytic cleavage of AURKB commonly occurs in other types of malignant tumor cells, including Burkitt's lymphoma (BL) and squamous cell carcinoma (SCC). Different in that only a major band (~35 kDa) of N-cleaved AURKB is observed in most KSHV-infected, EBV-infected, and HPV-infected cell lines, there are additional smaller cleaved products of AURKB that appeared in both primary KS and SCC tissues, which may be because primary cancer tissues are more complex than cell lines to some extent. In addition, we have attempted to detect the smaller cleaved N-terminal fragment of $AURKB_{(1–76aa)}$ at the endogenous level in the KSHV-positive B cell lines using an N terminus-specific AURKB antibody. Unfortunately, no protein band of the $AURKB_{(1–76aa)}$ form was observed, which could be due to protein instability.

Previous studies have shown that two splicing variant forms of AURKB exist in primary HCC tissues using RT-PCR analysis (Sistayanarain et al., 2006; Yasen et al., 2009) and a smaller immunoreactive protein of AURKB exists in HeLa cells (Honda et al., 2003). However, whether the splicing variants occur in other types of cancer cells and whether the smaller immunoreactive protein of AURKB in HeLa cells is due to the cause of transcriptional splicing or peptide cleavage remain unclear. In this study, we demonstrated that no splicing variants of AURKB at the post-transcriptional level occur in the KSHV-infected, EBV-infected, and HPV-infected cells using northern blot assay, and N-terminal

(B) Both endogenous C-cleaved and N-cleaved forms of AURKB localize at the centrosome during anaphase (scale bar, 5 μm). BCBL1 cells were subjected to immunofluorescence assay with antibodies against AURKB(N), AURKB(C), and tubulin. Nuclei are stained by DAPI. The centrosome is indicated by a box. Representative 3D images of BCBL1 cells with anti-AURKB(N) (green) and tubulin (red) staining can be viewed as still images or movies in Video S1.
(C) Knockdown of AURKA enhances the N and C cleavage of AURKB in PEL cells. Cell lysates from parental BCBL1 cells and its AURKA or scramble stable knockdown were subjected to immunoblotting (IB) analysis as indicated in the figure. Bottom: quantitation of AURKA knockdown efficiency is shown.

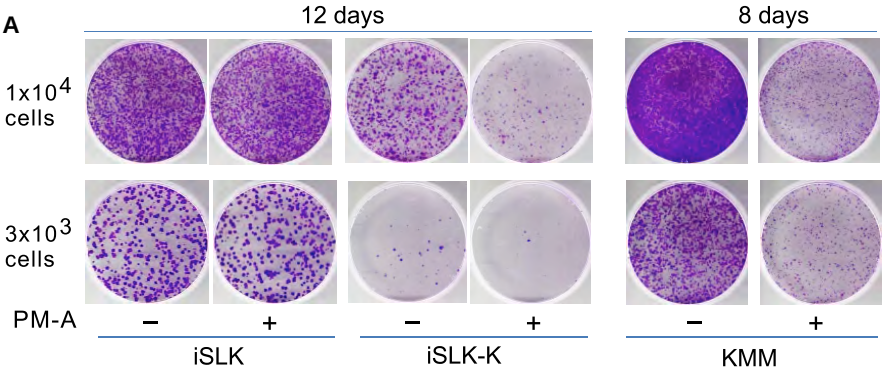

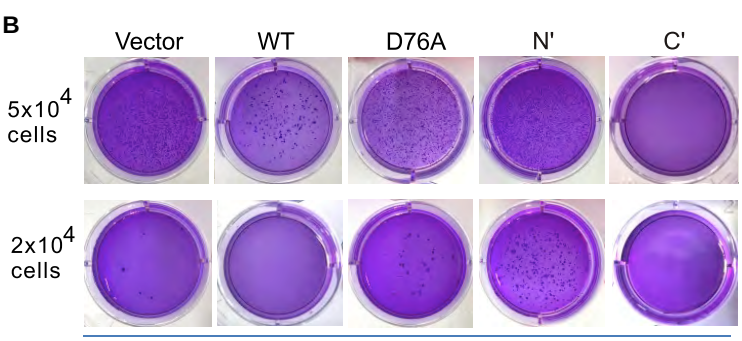

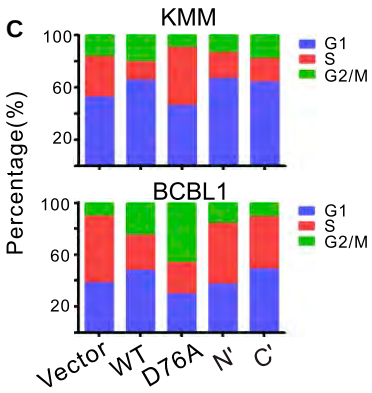

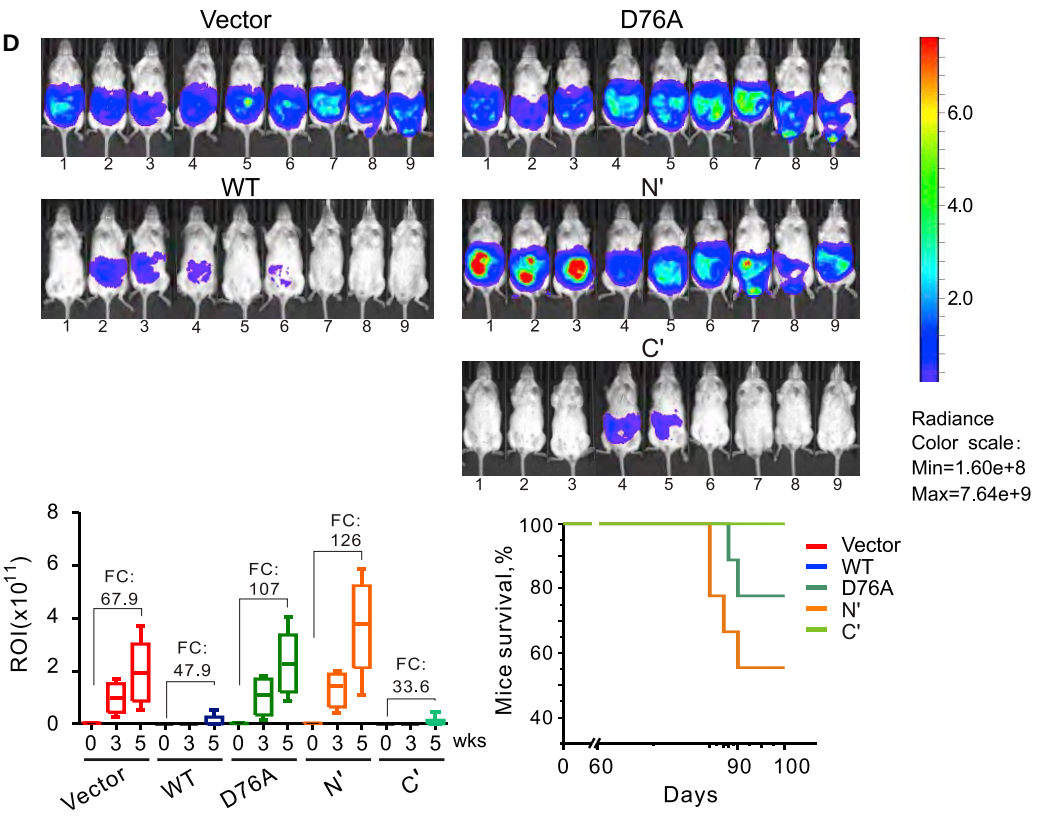

(legend on next page)

cleavage of AURKB at the post-translational level is consistently and highly induced upon infection of different cell types, including B lymphocyte and endothelial and epithelial cells, with various oncoviruses, particularly KSHV. Furthermore, the results of a previous report show that the level of AURKB expression is increased in SCC instead of NILM or ACS-US tissues (Twu et al., 2009). We also observed that the N′-AURKB more frequently occurs in SCC tissues compared to the C′-AURKB (10 of 10 versus 4 of 10 cases), and a strong correlation between the level of N′-AURKB (ratio with native AURKB) and metastasis in cervical cancer was observed. In contrast, although at least two splicing variants of AURKB have been reported in both primary HCC tissues and cell lines (Sistayanarain et al., 2006; Yasen et al., 2009), except for the 97H cell, only one band of N′-AURKB was consistently observed in the seven HCC cell lines, including Huh7 and HepG3B (no AURKB isoform was observed in these two cell lines in two previous studies; Sistayanarain et al., 2006; Yasen et al., 2009), and no C′-AURKB was detected in all eight cell lines (data not shown), indicating that the splicing variants of AURKB are not translated and may regulate only at the transcriptional level, not the translational level.

In terms of the cleavage site of AURKB induced by KSHV, the observation of a similar-molecular weight (~35 kDa) cleaved band of exogenous AURKB and AURKA with myc tag at their C termini, which was evidently pulled down by LANA, indicates that AURKB and AURKA share a homologous sequence at their C termini. This in turn prompted us to analyze the potential cleavage sites within The N termini of these two molecules by using online prediction software. We identified two potential cleavage sites at D76 and K85 in AURKB (D132 and K141 in AURKA) that are mediated by HIV retropepsin and trypsin, respectively. Site-directed mutation assays involving AURKB indicated that only the mutation involving D76 instead of K85 reduces LANA-induced AURKB cleavage, although the mutation of K85 results in cleavage of AURKB at D76 to some extent. Because the cleavage site of AURKB on D76 is located within an activation domain that is highly homologous to that in AURKA, there is no doubt that a similar-molecular weight cleaved form of AURKA at D132 was pulled down by LANA. However, distinct from AURKA, and to investigate AURKB cleavage at D76, the caspase-mediated cleavage site of AURKB at Asp^{75} was also identified, and the inhibitor of pan caspase instead of caspase-1 and caspase-3 and -7 could efficiently reduce the cleavage of AURKB at D76, indicating that N cleavage of AURKB is more important than that of AURKA during cell mitosis. Caspase-3 and -7 have been shown to be particularly involved in the cleavage of AURKB at M1, although the relative physiological function of this cleavage requires further investigation. In addition, the K106R mutant that inactivates AURKB function in mitosis abolishes LANA-induced cleavage of AURKB, indicating that the cleavage of AURKB is mainly confined to the process of mitosis, although the accurate stage remains to be investigated.

In accordance with the effect of LANA on N cleavage of AURKB, we observed that LANA is strongly associated with the C terminus of AURKB, and LANA has a higher affinity to the endogenous N′-cleaved product than intact AURKB in PEL cells. This in turn supports the notion that the association of LANA with the C terminus of AURKB induces the cleavage of AURKB at the N terminus. The co-expression of different N-terminal-cleaved mutants of exogenous AURKB, which harbors the LANA-binding region, dramatically induces LANA degradation (data not shown). This indicates that the reduction of LANA mediated by the C terminus of AURKB is probably a feedback mechanism that balances the LANA-induced cleavage of AURKB. Although caspase-1, caspase-3, and caspase-7 have been previously shown to induce the cleavage of LANA under oxidative stress (Davis et al., 2015), these do not involve in LANA-mediated cleavage of AURKB at D76, suggesting that LANA exerts a fine-tuning modulation under tumor microenvironmental stress.

In agreement with previous findings that AURKB mainly localizes at the inner centromere regions during prophase and subsequently relocalizes to the midzone of the central spindle and concentrates at the midbody (Adams et al., 2000; Kaitna et al., 2000; Terada et al., 1998), and that its catalytically inactive mutant K106R fails to drive cell segregation during mitosis (Honda et al., 2003), we observed that the ectopically expressed WT AURKB, instead of its K106R mutant, presents the expected relocalization from centromeres to the central spindle. Although several previous studies have shown that the function between AURKA and AURKB could be converted by manipulating their different localizations or even single amino acid change (Fu et al., 2009; Hans et al., 2009; Li et al., 2015), the cause of their conversion in physiological relevance remains to be investigated. In this study, we observed punctate signals of exogenous AURKB distributed in the poles of cells co-expressing LANA, as well as the spindle pole localization of endogenous AURKB forms in BCBL1 cells during mitosis, which is distinct from the typical distribution of AURKB. In particular,

Figure 7. N-Cleaved Form of AURKB Promotes Tumor Cells Growth *In Vitro* and *In Vivo*

(A) Serine protease inhibitors reduce the colony formation of KSHV latently infected cells *in vitro*. Equal amounts of iSLK, iSLK-K (KSHV), and KMM (KSHV) cells were individually inoculated and treated with or without serine protease inhibitors PM-A (PMSF-aprotinin) and subjected to colony formation assays as indicated. The cells were fixed 8 and 12 days later and stained with crystal violet to determine colony number.

(B) N-cleaved form of AURKB at Asp^{76} residue enhances colony formation of PEL cells in soft agar. Equal amounts of BCBL1 cells stably expressing YFP-tagged WT AURKB and its D76A, N-cleaved (N′), or C-cleaved (C′) mutant or vector alone were individually inoculated for soft agar assays and then fixed 21 days later, followed by staining with crystal violet to determine colony number.

(C) DNA content analysis of KMM and BCBL1 cells stably expressing YFP-tagged AURKB or vector alone. The percentage of G1, S, and G2/M populations was quantified from Figure S6D.

(D) N-cleaved form of AURKB on Asp^{76} enhances PEL tumor growth in a xenograft mouse model. The tumor burden of nine non-obese diabetic (NOD) and severe combined immunodeficiency (SCID) mice intraperitoneally engrafted with 10^7 BCBL1-Luc cells stably expressing WT AURKB and its D76A, N-cleaved (N′), or C-cleaved (C′) mutant or vector alone were analyzed at every week. Bottom: luminescent signals at weeks 0, 3, and 5 were quantified and expressed in region-of-interest (ROI) signal intensity [Total radiant efficiency(p/s)/(microwatts per square centimeter)]. Right: total percentage of survival mice in each group is shown. FC, fold change. Statistical significance is defined in STAR Methods (means ± SEM, n = 9 mice, t test).

the N′-AURKB or C′-AURKB can relocate to the pole where AURKA is concentrated during mitosis. These findings suggested that the punctate pole localization of AURKB may due to the cleaved forms of AURKB by LANA and that the N and C cleavage of AURKB is an alternative mechanism to function as an AURKA-like protein that drives mitotic cell progression. Knocking down endogenous AURKA results in a higher increase in C cleavage of endogenous AURKB in PEL cells, which supports our hypothesis. The results from time-lapse live-cell imaging reveal that the N′-AURKB and C′-AURKB products exert a fine-tuning mitotic control by modulating the transition time from different phases of mitosis. Distinct from the C′-AURKB that is exclusively located in the cytoplasm compartment, the N′-AURKB equally distributes in both nuclear and cytoplasm compartments. The serine protease inhibitors effectively block the nuclear localization of N′-AURKB, but not the cytoplasm localization of C′-AURKB, confirming that N cleavage of AURKB depends on the serine protease, and it may occur at the early stage of cell mitosis or interphase in which the nuclear compartment is retained.

It has been previously demonstrated that AURKA or AURKB is commonly overexpressed in many cancer cells, and overexpression of exogenous AURKA or AURKB could result in multinuclearity and aneuploidy due to failure of cell division (Giet et al., 2005). However, how the aberrantly high level of AURKA or AURKB expression is maintained and balanced to coordinate in driving mitotic cell progression and malignancy remains unclear. The observation that inhibiting N cleavage of AURKB significantly reduces cell proliferation and colony formation in KSHV-infected instead of uninfected cells *in vitro* indicates that N cleavage of AURKB contributes to cell growth. In B cells or endothelial cells, the N′-cleaved form of AURKB consistently drives higher colony formation *in vitro*, but it did not result in a significant change in cell-cycle populations compared to WT AURKB or vector alone. The mechanism underlying how N′-AURKB accelerates PEL tumor growth remains to be investigated.

BCBL1 cells carrying D76A mutant is assumed to be less than AURKB-WT in colony formation *in vitro*; however, the actual effect we observed is opposite and distinct from the growth-inhibitory effects of D76A mutation in endothelial cells. The cell-cycle analysis shows a more than 3-fold increase in the subG1 (cell death and apoptosis) population of BCBL1-AURKB-D76A compared with BCBL1-AURKB-WT, which is highly caused by failure mitosis once the overexpressed AURKB couldn't be effectively cleaved in BCBL1 cells. In addition, there are high-level populations of BCBL1-AURKB-D76A distributed in the G2/M phase. One possible explanation is that a portion of BCBL1 cells carrying D76A mutant, with high probability, have adapted an unknown mechanism to overcome mitosis obstructions, leading to rapid entry into mitosis during passage. This reflects that AURKB cleavage is essential for effective mitosis in certain cancer cells. Otherwise, an adaptive survival mechanism in cancer cell may have evolved that accelerates tumor growth.

In summary, consistent with the observation of colony formation *in vitro*, the N′-cleaved form of AURKB drives the highest tumor growth and malignancy *in vivo*, indicating that N cleavage of AURKB enhances cell segregation and tumorigenesis and may be potentially used as a target for cancer diagnosis and therapy.

STAR★METHODS

Detailed methods are provided in the online version of this paper and include the following:

- KEY RESOURCES TABLE
- CONTACT FOR REAGENT AND RESOURCE SHARING
- EXPERIMENTAL MODEL AND SUBJECT DETAILS
  - Human Subjects
  - Cell Lines
  - Animals
- METHOD DETAILS
  - Antibodies and Reagents
  - Cell Transfection
  - DNA Constructs
  - Co-IP and IB
  - Live Cell Imaging
  - Cell Cycle Assay
  - Immunofluorescence Analysis
  - Subcellular Fractionation
  - Generation of Cell Lines with Stable Expression
  - Colony Formation and Cell proliferation assays
  - Northern blotting
  - KSHV virion purification and primary infection
  - Tumor xenograft
- QUANTIFICATION AND STATISTICAL ANALYSIS
- DATA AND SOFTWARE AVAILABILITY

SUPPLEMENTAL INFORMATION

Supplemental Information can be found with this article online at https://doi.org/10.1016/j.celrep.2019.02.106.

ACKNOWLEDGMENTS

We are grateful to Erich Nigg from Max-Planck Institute of Biochemistry, Shou-Jiang Gao from University of Pittsburgh, and Erle Robertson from University of Pennsylvania for providing reagents. This work was supported by the National Natural Science Foundation of China (81672015 and 81471930 to Q.C., 81772166 to F.W., and 81501739 to C.Z.) and the National Key Research and Development Program of China (2016YFC1200400 to Q.C.). Q.C. is a scholar of New Century Excellent Talents in University of China.

AUTHOR CONTRIBUTIONS

Q.Z., F.W., and Q.C. designed the experiments, analyzed and organized data, and wrote the paper; Q.Z., L.D., and Z.Z. performed the experiments; C.W., Y.W., and C.Z. helped construct mutants and small hairpin RNAs (shRNAs); and S.G. and Z.Y. provided patient tissue samples and reagents. All authors discussed the results and commented on the manuscript.

DECLARATION OF INTERESTS

The authors declare no competing interests.

Received: October 20, 2018
Revised: January 4, 2019
Accepted: February 27, 2019
Published: March 26, 2019; corrected online April 25, 2019

REFERENCES

Adams, R.R., Wheatley, S.P., Gouldsworthy, A.M., Kandels-Lewis, S.E., Carmena, M., Smythe, C., Gerloff, D.L., and Earnshaw, W.C. (2000). INCENP binds the Aurora-related kinase AIRK2 and is required to target it to chromosomes, the central spindle and cleavage furrow. Curr. Biol. *10*, 1075–1078.

Ballestas, M.E., Chatis, P.A., and Kaye, K.M. (1999). Efficient persistence of extrachromosomal KSHV DNA mediated by latency-associated nuclear antigen. Science *284*, 641–644.

Ban, R., Nishida, T., and Urano, T. (2011). Mitotic kinase Aurora-B is regulated by SUMO-2/3 conjugation/deconjugation during mitosis. Genes Cells *16*, 652–669.

Brown, J.R., Koretke, K.K., Birkeland, M.L., Sanseau, P., and Patrick, D.R. (2004). Evolutionary relationships of Aurora kinases: implications for model organism studies and the development of anti-cancer drugs. BMC Evol. Biol. *4*, 39.

Brulois, K.F., Chang, H., Lee, A.S., Ensser, A., Wong, L.Y., Toth, Z., Lee, S.H., Lee, H.R., Myoung, J., Ganem, D., et al. (2012). Construction and manipulation of a new Kaposi's sarcoma-associated herpesvirus bacterial artificial chromosome clone. J. Virol. *86*, 9708–9720.

Cai, Q.L., Knight, J.S., Verma, S.C., Zald, P., and Robertson, E.S. (2006). EC5S ubiquitin complex is recruited by KSHV latent antigen LANA for degradation of the VHL and p53 tumor suppressors. PLoS Pathog. *2*, e116.

Cai, Q., Xiao, B., Si, H., Cervini, A., Gao, J., Lu, J., Upadhyay, S.K., Verma, S.C., and Robertson, E.S. (2012). Kaposi's sarcoma herpesvirus upregulates Aurora A expression to promote p53 phosphorylation and ubiquitylation. PLoS Pathog. *8*, e1002566.

Carmena, M., and Earnshaw, W.C. (2003). The cellular geography of aurora kinases. Nat. Rev. Mol. Cell Biol. *4*, 842–854.

Carmena, M., Wheelock, M., Funabiki, H., and Earnshaw, W.C. (2012). The chromosomal passenger complex (CPC): from easy rider to the godfather of mitosis. Nat. Rev. Mol. Cell Biol. *13*, 789–803.

Cheetham, G.M., Knegtel, R.M., Coll, J.T., Renwick, S.B., Swenson, L., Weber, P., Lippke, J.A., and Austen, D.A. (2002). Crystal structure of aurora-2, an oncogenic serine/threonine kinase. J. Biol. Chem. *277*, 42419–42422.

Chen, L., and Lagunoff, M. (2005). Establishment and maintenance of Kaposi's sarcoma-associated herpesvirus latency in B cells. J. Virol. *79*, 14383–14391.

Cotter, M.A., 2nd, Subramanian, C., and Robertson, E.S. (2001). The Kaposi's sarcoma-associated herpesvirus latency-associated nuclear antigen binds to specific sequences at the left end of the viral genome through its carboxy-terminus. Virology *291*, 241–259.

Davis, D.A., Naiman, N.E., Wang, V., Shrestha, P., Haque, M., Hu, D., Anagho, H.A., Carey, R.F., Davidoff, K.S., and Yarchoan, R. (2015). Identification of Caspase Cleavage Sites in KSHV Latency-Associated Nuclear Antigen and Their Effects on Caspase-Related Host Defense Responses. PLoS Pathog. *11*, e1005064.

Emanuele, M.J., Lan, W., Jwa, M., Miller, S.A., Chan, C.S., and Stukenberg, P.T. (2008). Aurora B kinase and protein phosphatase 1 have opposing roles in modulating kinetochore assembly. J. Cell Biol. *181*, 241–254.

Fernández-Miranda, G., Pérez de Castro, I., Carmena, M., Aguirre-Portolés, C., Ruchaud, S., Fant, X., Montoya, G., Earnshaw, W.C., and Malumbres, M. (2010). SUMOylation modulates the function of Aurora-B kinase. J. Cell Sci. *123*, 2823–2833.

Fu, J., Bian, M., Jiang, Q., and Zhang, C. (2007). Roles of Aurora kinases in mitosis and tumorigenesis. Mol. Cancer Res. *5*, 1–10.

Fu, J., Bian, M., Liu, J., Jiang, Q., and Zhang, C. (2009). A single amino acid change converts Aurora-A into Aurora-B-like kinase in terms of partner specificity and cellular function. Proc. Natl. Acad. Sci. USA *106*, 6939–6944.

Gantt, S., and Casper, C. (2011). Human herpesvirus 8-associated neoplasms: the roles of viral replication and antiviral treatment. Curr. Opin. Infect. Dis. *24*, 295–301.

Giet, R., Petretti, C., and Prigent, C. (2005). Aurora kinases, aneuploidy and cancer, a coincidence or a real link? Trends Cell Biol. *15*, 241–250.

González-Loyola, A., Fernández-Miranda, G., Trakala, M., Partida, D., Samejima, K., Ogawa, H., Cañamero, M., de Martino, A., Martínez-Ramírez, Á., de Cárcer, G., et al. (2015). Aurora B Overexpression Causes Aneuploidy and p21Cip1 Repression during Tumor Development. Mol. Cell. Biol. *35*, 3566–3578.

Goto, H., Yasui, Y., Nigg, E.A., and Inagaki, M. (2002). Aurora-B phosphorylates Histone H3 at serine28 with regard to the mitotic chromosome condensation. Genes Cells *7*, 11–17.

Gruneberg, U., Neef, R., Honda, R., Nigg, E.A., and Barr, F.A. (2004). Relocation of Aurora B from centromeres to the central spindle at the metaphase to anaphase transition requires MKlp2. J. Cell Biol. *166*, 167–172.

Gully, C.P., Velazquez-Torres, G., Shin, J.H., Fuentes-Mattei, E., Wang, E., Carlock, C., Chen, J., Rothenberg, D., Adams, H.P., Choi, H.H., et al. (2012). Aurora B kinase phosphorylates and instigates degradation of p53. Proc. Natl. Acad. Sci. USA *109*, E1513–E1522.

Hans, F., Skoufias, D.A., Dimitrov, S., and Margolis, R.L. (2009). Molecular distinctions between Aurora A and B: a single residue change transforms Aurora A into correctly localized and functional Aurora B. Mol. Biol. Cell *20*, 3491–3502.

He, M., Tan, B., Vasan, K., Yuan, H., Cheng, F., Ramos da Silva, S., Lu, C., and Gao, S.J. (2017). SIRT1 and AMPK pathways are essential for the proliferation and survival of primary effusion lymphoma cells. J. Pathol. *242*, 309–321.

Honda, R., Körner, R., and Nigg, E.A. (2003). Exploring the functional interactions between Aurora B, INCENP, and survivin in mitosis. Mol. Biol. Cell *14*, 3325–3341.

Jha, H.C., Upadhyay, S.K., A J Prasad, M., Lu, J., Cai, Q., Saha, A., and Robertson, E.S. (2013). H2AX phosphorylation is important for LANA-mediated Kaposi's sarcoma-associated herpesvirus episome persistence. J. Virol. *87*, 5255–5269.

Jones, T., Ye, F., Bedolla, R., Huang, Y., Meng, J., Qian, L., Pan, H., Zhou, F., Moody, R., Wagner, B., et al. (2012). Direct and efficient cellular transformation of primary rat mesenchymal precursor cells by KSHV. J. Clin. Invest. *122*, 1076–1081.

Kaitna, S., Mendoza, M., Jantsch-Plunger, V., and Glotzer, M. (2000). Incenp and an aurora-like kinase form a complex essential for chromosome segregation and efficient completion of cytokinesis. Curr. Biol. *10*, 1172–1181.

Kakuguchi, W., Kitamura, T., Kuroshima, T., Ishikawa, M., Kitagawa, Y., Totsuka, Y., Shindoh, M., and Higashino, F. (2010). HuR knockdown changes the oncogenic potential of oral cancer cells. Mol. Cancer Res. *8*, 520–528.

King, R.W., Glotzer, M., and Kirschner, M.W. (1996). Mutagenic analysis of the destruction signal of mitotic cyclins and structural characterization of ubiquitinated intermediates. Mol. Biol. Cell *7*, 1343–1357.

Knowlton, A.L., Lan, W., and Stukenberg, P.T. (2006). Aurora B is enriched at merotelic attachment sites, where it regulates MCAK. Curr. Biol. *16*, 1705–1710.

Krupina, K., Kleiss, C., Metzger, T., Fournane, S., Schmucker, S., Hofmann, K., Fischer, B., Paul, N., Porter, I.M., Raffelsberger, W., et al. (2016). Ubiquitin Receptor Protein UBASH3B Drives Aurora B Recruitment to Mitotic Microtubules. Dev. Cell *36*, 63–78.

Kumar, S., van Raam, B.J., Salvesen, G.S., and Cieplak, P. (2014). Caspase cleavage sites in the human proteome: CaspDB, a database of predicted substrates. PLoS ONE *9*, e110539.

Li, S., Deng, Z., Fu, J., Xu, C., Xin, G., Wu, Z., Luo, J., Wang, G., Zhang, S., Zhang, B., et al. (2015). Spatial Compartmentalization Specializes the Function of Aurora A and Aurora B. J. Biol. Chem. *290*, 17546–17558.

López-Saavedra, A., and Herrera, L.A. (2010). The role of alternative mRNA splicing in chromosome instability. Mutat. Res. *705*, 246–251.

Lu, J., Jha, H.C., Verma, S.C., Sun, Z., Banerjee, S., Dzeng, R., and Robertson, E.S. (2014). Kaposi's sarcoma-associated herpesvirus-encoded LANA contributes to viral latent replication by activating phosphorylation of survivin. J. Virol. *88*, 4204–4217.

Mo, X., Wei, F., Tong, Y., Ding, L., Zhu, Q., Du, S., Tan, F., Zhu, C., Wang, Y., Yu, Q., et al. (2018). Lactic Acid Downregulates Viral MicroRNA To Promote

Epstein-Barr Virus-Immortalized B Lymphoblastic Cell Adhesion and Growth. J. Virol. *92*, e00033-18.

Nascimento, R., Costa, H., and Parkhouse, R.M. (2012). Virus manipulation of cell cycle. Protoplasma *249*, 519–528.

Nguyen, H.G., Chinnappan, D., Urano, T., and Ravid, K. (2005). Mechanism of Aurora-B degradation and its dependency on intact KEN and A-boxes: identification of an aneuploidy-promoting property. Mol. Cell. Biol. *25*, 4977–4992.

Nigg, E.A. (2001). Mitotic kinases as regulators of cell division and its checkpoints. Nat. Rev. Mol. Cell Biol. *2*, 21–32.

Pan, H., Zhou, F., and Gao, S.J. (2004). Kaposi's sarcoma-associated herpesvirus induction of chromosome instability in primary human endothelial cells. Cancer Res. *64*, 4064–4068.

Rawlings, N.D., Barrett, A.J., Thomas, P.D., Huang, X., Bateman, A., and Finn, R.D. (2018). The MEROPS database of proteolytic enzymes, their substrates and inhibitors in 2017 and a comparison with peptidases in the PANTHER database. Nucleic Acids Res. *46* (*D1*), D624–D632.

Saha, A., Halder, S., Upadhyay, S.K., Lu, J., Kumar, P., Murakami, M., Cai, Q., and Robertson, E.S. (2011). Epstein-Barr virus nuclear antigen 3C facilitates G1-S transition by stabilizing and enhancing the function of cyclin D1. PLoS Pathog. *7*, e1001275.

Schilling, O., and Overall, C.M. (2008). Proteome-derived, database-searchable peptide libraries for identifying protease cleavage sites. Nat. Biotechnol. *26*, 685–694.

Si, H., and Robertson, E.S. (2006). Kaposi's sarcoma-associated herpesvirus-encoded latency-associated nuclear antigen induces chromosomal instability through inhibition of p53 function. J. Virol. *80*, 697–709.

Sistayanarain, A., Tsuneyama, K., Zheng, H., Takahashi, H., Nomoto, K., Cheng, C., Murai, Y., Tanaka, A., and Takano, Y. (2006). Expression of Aurora-B kinase and phosphorylated histone H3 in hepatocellular carcinoma. Anticancer Res. *26* (*5A*), 3585–3593.

Stewart, S., and Fang, G. (2005). Destruction box-dependent degradation of aurora B is mediated by the anaphase-promoting complex/cyclosome and Cdh1. Cancer Res. *65*, 8730–8735.

Sugiyama, K., Sugiura, K., Hara, T., Sugimoto, K., Shima, H., Honda, K., Furukawa, K., Yamashita, S., and Urano, T. (2002). Aurora-B associated protein phosphatases as negative regulators of kinase activation. Oncogene *21*, 3103–3111.

Sumara, I., Quadroni, M., Frei, C., Olma, M.H., Sumara, G., Ricci, R., and Peter, M. (2007). A Cul3-based E3 ligase removes Aurora B from mitotic chromosomes, regulating mitotic progression and completion of cytokinesis in human cells. Dev. Cell *12*, 887–900.

Takeshita, M., Koga, T., Takayama, K., Ijichi, K., Yano, T., Maehara, Y., Nakanishi, Y., and Sueishi, K. (2013). Aurora-B overexpression is correlated with aneuploidy and poor prognosis in non-small cell lung cancer. Lung Cancer *80*, 85–90.

Terada, Y. (2001). Role of chromosomal passenger complex in chromosome segregation and cytokinesis. Cell Struct. Funct. *26*, 653–657.

Terada, Y., Tatsuka, M., Suzuki, F., Yasuda, Y., Fujita, S., and Otsu, M. (1998). AIM-1: a mammalian midbody-associated protein required for cytokinesis. EMBO J. *17*, 667–676.

Twu, N.F., Yuan, C.C., Yen, M.S., Lai, C.R., Chao, K.C., Wang, P.H., Wu, H.H., and Chen, Y.J. (2009). Expression of Aurora kinase A and B in normal and malignant cervical tissue: high Aurora A kinase expression in squamous cervical cancer. Eur. J. Obstet. Gynecol. Reprod. Biol. *142*, 57–63.

Verma, S.C., Borah, S., and Robertson, E.S. (2004). Latency-associated nuclear antigen of Kaposi's sarcoma-associated herpesvirus up-regulates transcription of human telomerase reverse transcriptase promoter through interaction with transcription factor Sp1. J. Virol. *78*, 10348–10359.

Wang, C., Zhu, C., Wei, F., Gao, S., Zhang, L., Li, Y., Feng, Y., Tong, Y., Xu, J., Wang, B., et al. (2017). Nuclear Localization and Cleavage of STAT6 Is Induced by Kaposi's Sarcoma-Associated Herpesvirus for Viral Latency. PLoS Pathog. *13*, e1006124.

Wei, F., Gan, J., Wang, C., Zhu, C., and Cai, Q. (2016). Cell Cycle Regulatory Functions of the KSHV Oncoprotein LANA. Front. Microbiol. *7*, 334.

Xiao, B., Verma, S.C., Cai, Q., Kaul, R., Lu, J., Saha, A., and Robertson, E.S. (2010). Bub1 and CENP-F can contribute to Kaposi's sarcoma-associated herpesvirus genome persistence by targeting LANA to kinetochores. J. Virol. *84*, 9718–9732.

Yasen, M., Mizushima, H., Mogushi, K., Obulhasim, G., Miyaguchi, K., Inoue, K., Nakahara, I., Ohta, T., Aihara, A., Tanaka, S., et al. (2009). Expression of Aurora B and alternative variant forms in hepatocellular carcinoma and adjacent tissue. Cancer Sci. *100*, 472–480.

Yasui, Y., Urano, T., Kawajiri, A., Nagata, K., Tatsuka, M., Saya, H., Furukawa, K., Takahashi, T., Izawa, I., and Inagaki, M. (2004). Autophosphorylation of a newly identified site of Aurora-B is indispensable for cytokinesis. J. Biol. Chem. *279*, 12997–13003.

Ye, F.C., Zhou, F.C., Yoo, S.M., Xie, J.P., Browning, P.J., and Gao, S.J. (2004). Disruption of Kaposi's sarcoma-associated herpesvirus latent nuclear antigen leads to abortive episome persistence. J. Virol. *78*, 11121–11129.

STAR★METHODS

KEY RESOURCES TABLE

REAGENT or RESOURCE	SOURCE	IDENTIFIER
Antibodies		
Rabbit monoclonal anti-AURKB-N	Abcam	Cat.#:EP1009Y
Rabbit polyclonal anti-AURKB-C	Abcam	Cat.#:Ab70238
Rabbit monoclonal anti-α tubulin	Proteintech	Cat.#:66031-1-Ig
Rabbit monoclonal anti-Histone H3	Cell Signaling Technology	Cat.#:9715
Mouse monoclonal anti-EBNA1	Santa cruz	Cat.#:sc-57719
Mouse monoclonal anti-GFP	Santa cruz	Cat.#: sc-53882
Mouse monoclonal anti-FLAG (M2)	Sigma-Aldrich	Cat.#:F1804
Mouse monoclonal anti-myc (9E10)	Lab stored	N/A
Mouse monoclonal anti-LANA1	Lab stored	N/A
Alexa Fluor® 488 Goat anti-Rabbit	Jackson immunoResearch	Cat. #:111-545-44
Alexa Fluor® 594 Goat anti-Mouse	Jackson immunoResearch	Cat. #:115-585-166
IRDye® 800cw Goat Anti-Mouse IgG	Li-COR	Cat. #: 926-32210
IRDye® 800cw Goat Anti-Rabbit IgG	Li-COR	Cat. #: 926-32211
Bacterial and Virus Strains		
KSHV (Bac16)	Lab stored	Brulois et al., 2012
Epstein-Barr Virus (B95.8)	Lab stored	Mo et al., 2018
Chemicals, Peptides, and Recombinant Proteins		
PMSF	Amresco	Cat. #:329-98-6
Aprotinin	Amresco	Cat. #:9087-70-1
Leupeptin	Amresco	Cat. #:103476-89-7
Pepstatin	Amresco	Cat. #:26305-03-3
MG132	Biomolecule Intl.	Cat. #:133407-826
Z-VAD-FMK	TargetMol	Cat. #:187389-52-2
Z-DEVD-FMK	TargetMol	Cat. #:210344-95-9
Ac-YVAD-CHO	Santa Cruz	Cat. #:143313-51-3
XenoLight D-Luciferin-K+	PerkinElmer	Cat. #:122799
Propidium iodide	Sigma-Aldrich	Cat.#:p4170
polyethyleneimine	Polyscience Inc	Cat.#:23966
Deposited Data		
Raw data	This paper	https://doi.org/10.17632/s5d8fkzwhj.1
Experimental Models: Cell Lines		
HeLa cells	ATCC(American type culture collection)	Cat.#:CCL-2
HEK293T cells	CCTCC (China Center for Type Culture Collection)	GDC187
iSLK cells	Gao SJ Lab	Brulois et al., 2012
iSLK-Bac16 cells	Gao SJ Lab	Brulois et al., 2012
KMM cells	Gao SJ Lab	Jones et al., 2012
HUVECs	ATCC (American type culture collection)	Cat.#:CRL-1730
BJAB cells	Robertson ES Lab	Cai et al., 2006
K-BJAB cells	Lagunoff M Lab	Chen and Lagunoff, 2005
BCBL1	Robertson ES Lab	Cai et al., 2006
BC3	ATCC(American type culture collection)	Cat.#:CRL-2277
JSC1	ATCC(American type culture collection)	Cat.#:CRL-2769
BL41	Robertson ES Lab	Saha et al., 2011

(*Continued on next page*)

Continued

REAGENT or RESOURCE	SOURCE	IDENTIFIER
BL41.B95.8	Robertson ES Lab	Saha et al., 2011
LCL	Lab stored	Mo et al., 2018
B95.8	ATCC (American type culture collection)	Cat. #: CRL-1612
Caski	ATCC (American type culture collection)	Cat. #: CRL-1550
C33A	ATCC (American type culture collection)	Cat. #: HTB-31
Oligonucleotides		
Table S1	This paper	N/A
Recombinant DNA		
pEGFP-C1-AURKB(1-109)	This paper	N/A
pEGFP-C1-AURKB(1-76)	This paper	N/A
pEGFP-C1-AURKB(1-195)	This paper	N/A
pEGFP-C1-AURKB(77-end)	This paper	N/A
pEGFP-C1-AURKB(109-end)	This paper	N/A
pEGFP-C1-AURKB(250-end)	This paper	N/A
pEGFP-C1-AURKB(290-end)	This paper	N/A
pEGFP-C1-AURKB-D76R	This paper	N/A
pEGFP-C1-AURKB-D76A	This paper	N/A
pEGFP-C1-AURKB-K85A	This paper	N/A
pEGFP-C1-AURKB-D76A,K85A	This paper	N/A
pEGFP-C1-AURKB-K106R	This paper	N/A
pEGFP-C1-AURKA-K162R	This paper	N/A
pLVX-YFP-AURKB (1-344)	This paper	N/A
pLVX-YFP-AURKB(1-250)	This paper	N/A
pLVX-YFP-AURKB-(77-end)	This paper	N/A
pLVX-YFP-AURKB- D76A	This paper	N/A
pmCherry-C1-AURKA(1-403)	This paper	N/A
Software and Algorithms		
FlowJo v10	FlowJo, LLC	https://www.flowjo.com/
GraphPad Prism 5	GraphPad Software	https://www.graphpad.com/
SoftWoRx Explorer	Applied Precision,Inc	https://www.gelifesciences.com/en/us/shop/cell-imaging-and-analysis/high-and-super-resolution-microscopes
Living Image 4.3 software	PerkinElmer	http://www.perkinelmer.com/

CONTACT FOR REAGENT AND RESOURCE SHARING

Further information and requests for resources and reagents should be directed to and will be fulfilled by the Lead Contact, Qiliang Cai (qiliang@fudan.edu.cn).

EXPERIMENTAL MODEL AND SUBJECT DETAILS

Human Subjects

Cervical tissues from female patients (age 24 to 69) diagnosed with HR-HPV negative for intraepithelial lesion or malignancy (NILM, HPV-), atypical squamous cells of undetermined significance (ASC-US, HPV+) or squamous cell carcinoma (SCC, HPV+) were all collected from Hospital and Institute of Obstetrics and Gynecology, Shanghai Medical College, Fudan University. KS tissue samples from male patients (age 45 to 60) were provided by Shanghai Public Health Clinical Center. Usage of redundant cancer sample for research purpose was approved by the Hospital Medical Ethics Committee. The IRB approved protocol in which Declaration of Helsinki protocols were followed and each donor gave written, informed consent. Sample size was based on feasibility and availability of human excess tissue collections.

Cell Lines

HeLa (isolated from female patient, American type culture collection, ATCC), Caski (isolated from female patient, ATCC), C33A (isolated from female patient, ATCC) and HEK293T (the sex information was not available, ATCC) were maintained in DMEM supplemented with 7% FBS and 1% Penicillin (Sangon Biotech) and Streptomycin (BBI Life Sciences). KSHV negative iSLK (the sex information was not available, 1ug/ml Puromycin, 250ug/ml G418) and KSHV positive iSLK-Bac16 (1.2mg/ml Hygromycin, 1 μg/ml Puromycin, 250ug/ml G418, kindly provided by Shou-Jiang Gao from University of Pittsburgh) cells were maintained in DMEM supplemented with 7% FBS (Brulois et al., 2012). KSHV negative MM (the sex information was not available) and KSHV positive KMM cells (kindly provided by Shou-Jiang Gao from University of Pittsburgh) were maintained in 10% FBS contained DMEM (Jones et al., 2012). HUVECs (the sex information was not available) were cultured with RPMI 1640 medium containing 10%FBS.

KSHV-negative BJAB (isolated from female patient, ATCC) and KSHV-positive BCBL1(the sex information was not available), BC3 (isolated from male patient), and JSC-1 (isolated from male patient, ATCC) B-lymphoma cells and K-BJAB, EBV-negative BL41 (the sex information was not available) and EBV-positive BL41.B95.8, and LCL (isolated from male patient) were maintained in RPMI1640 medium supplemented with 10% FBS and 1% Penicillin and Streptomycin as described previously (Cai et al., 2006; Chen and Lagunoff, 2005; Mo et al., 2018; Saha et al., 2011). All cell lines were incubated at 37°C in humidified environmental incubator with 5% CO_2.

Animals

Ethics Statement and Husbandry

All animal studies were conducted in accordance with China guide for the Care and Use of Laboratory Animals. All experiments were approved and overseen by the institutional animal care and use committee at Fudan University under Protocol ID 196086. Five-week-old female NOD/SCID mice were purchased from Beijing Vital River Laboratory Animal Technology Co., Ltd (Beijing, China). Mice were housed in microisolator cages with no more than 5 mice per cage at certified specific-pathogen-free or germ-free vivaria. Animals had access to autoclaved water and food *ad libitum*.

METHOD DETAILS

Antibodies and Reagents

Antibodies against AURKB-N (EP1009Y, Abcam), AURKB-C (ab70238, Abcam), a-tubulin (Proteintech), Histone H3 (cell signaling), FLAG (M2, Sigma), and GAPDH (Proteintech) were used according to the manufacture's instruction. The monoclonal antibodies against myc (9E10) and LANA (LANA1) were individually prepared from hybridoma cultures.

Protease inhibitors PMSF, Aprotinin, Leupeptin and Pepstatin A were purchased from Amresco. Proteasome inhibitor MG132 was purchased from Biomol International. Caspase inhibitors Z-VAD-FMK, Z-DEVD-FMK from TargetMol, and Ac-YVAD-CHO from Santa Cruz Biotechnology were purchased. XenoLight D-Luciferin-K+ Salt Bioluminescent Substrate were from PerkinElmer. Propidium iodide was purchased from Sigma.

Cell Transfection

HEK293T cells were transfected with 1mg/ml polyethyleneimine (PEI) at a ratio of 1 μg plasmid DNA: 3 μL PEI. HeLa cells transfection was performed with Lonza-4D nucleofector system in an optimized program.

DNA Constructs

Plasmid expression AURKB truncation mutants 1-250aa, 1-195aa, 1-109aa and 1-76aa were individually obtained by PCR-directed site mutation with pEGFP-C1-AURKB-WT (1-344) as template, and the AURKB truncation mutants 77-344aa, 109-344aa, 250-344aa and 290-344aa were constructed by PCR amplicon (AURKB-myc as template) inserted into pEGFP-C1 with restriction enzymes BamHI and KpnI, respectively. AURKB site mutants D76R, D76A, K85A and D76AK85A were individually constructed by PCR-directed site mutation with pEGFP-C1-AURKB-1-344 as template. The expression plasmids pLVX-YFP-AURKB-WT, pLVX-YFP-AURKB-1-250, pLVX-YFP-AURKB-77-344 and pLVX-YFP-AURKB-D76A were constructed by PCR amplicon inserted into pLVX-YFP vector (modified from pLVX-Puro) with restriction enzymes EcoRI and BamHI. pcDNA4(TO/myc-His)-AURK A/B WT and kinase inactive KR mutant (K162R for AURKA, K106R for AURKB) were provided by Erich A. Nigg from Max-Planck Institute of Biochemistry (Martinsried, Germany). Plasmids expressing LANA-FLAG, RFP-LANA, pcDNA3.1-GFP-NLS-myc and pGIPz-shAURKA were described previously (Cai et al., 2012; Verma et al., 2004).

Co-IP and IB

Cells (at least $15x10^6$) were harvested, washed twice with ice-cold PBS, and lysed in ice-cold RIPA (150mM NaCl, 50mM Tris pH7.6, 1% Nonidet P-40, 2mM EDTA with or without 1mM PMSF, 1g/ml Aprotinin, 1g/ml Leupeptin and 1g/ml Pepstatin) for 30min on ice with brief vortexing every 5 min. The lysates were centrifuged at 14,500 rpm for 5 min at 4°C to remove cell debris. Five percent of the supernatant was used as input. The rest supernatant was then incubated with the indicated primary antibody at 4°C with rotation overnight. Next day the supernatants were incubated with 35 μL protein A/G Sepharose beads (GE Co.) at 4°C with rotation for another 3 hr. For immunoblotting assays, the immunoprecipitates were boiled in 6x SDS loading buffer. The protein were separated

by SDS-PAGE and transferred to 0.45-mm nitrocellulose membrane for immunoblotting with primary antibodies and appropriate secondary antibodies. The member was scanned with an Odyssey Infrared scanner (Li-Cor Biosciences).

Live Cell Imaging

Approximately 6x10^5 293T cells were seeded into each well of 4-chamer Glass Bottom Dish (*In vitro* scientific) and individually transfected with GFP-AURKB or GFP-AURKB mutants in the presence or absence of RFP-LANA. At 24 h post-transfection, scattering distributed 293T cells expressing GFP or RFP were selected and filmed on Delta Vision high-resolution cell imaging systems (GE company) for 24 h. The chamber was maintained at 37°C and supplement with 5% CO_2 with a microscope stage heater. Images were captured in 5 or 7 minute interval.

Cell Cycle Assay

For imaging cell cycle assays, 293T cells with GFP-AURKB, GFP-AURKB K to R mutation, GFP-AURKA, or GFP-AURKA K to R mutation with RFP or RFP-LANA co-expression were performed by transient transfection. 2x10^4 cells were harvested and washed with ice-cold PBS, and then fixed with 70% ethanol and stained with DAPI solution for 5 min at room temperature in dark. Cell cycle phase and polynucleated cells were characterized by using ImageStreamX® MKII Imaging Flow Cytometer (Amnis EMD Millipore). GFP and RFP double positive cells were photographed and analyzed. For PI-staining cell cycle assay, the stable cell lines were harvested, washed twice with PBS and resuspended at 1x10^6 cells/ml. Aliquot 1ml cells in 15ml polypropylene, V-bottomed tube and add 3ml cold absolute ethanol. The cells were fixed in 70% ethanol at least 2 h at 4°C with rotation. The fixed cells were washed twice with PBS, and then 1ml propidium iodide (PI) staining solution (50ug/ml) and RNase A were added to cell pellet. The mixture was incubated 20min at room temperature. The 1.5x10^4 PI-stained cells were subject to flow cytometry by using BD FACS Calibur. The data were analyzed by FlowJo software.

Immunofluorescence Analysis

Immunofluorescence assays were performed as described previously with modification(Wang et al., 2017). Briefly, BCBL1 cell were harvested and fixed in 4% paraformaldehyde for 20 min in dark at room temperature, and then washed with PBS twice and resuspension with PBS. The fixed cells were spread evenly on 0.1% gelatin-treated coverslips and dying for 15min at 37°C incubator. Then cells were washed three times with blocking buffer PBS containing 0.2% fish skin gelatin (G-7765; Sigma) and 0.02% Triton X-100, and permeabilized in blocking buffer, followed by primary and secondary antibodies (goat&mouse 594 and goat &Rabbit 1:500) staining. Nucleus was stained with 4, 6-diamidino-2-phenylindole (DAPI), and coverslips were mounted with *p*-phenylenediamine. Cells in mitosis with separated chromosome were visualized with Leica SP8 confocal microscope.

Subcellular Fractionation

Preparation of nuclear or cytoplasm protein were performed as described previously(Wang et al., 2017). Briefly, at least 15x10^6 cells pellets were resuspension and lysis in buffer A (10mM HEPES-K+ pH7.5, 10mM KCl, 1.5mM MgCl2, with protease inhibitors) containing 0.1% NP-40 for 5min on ice after a cold PBS wash. Homogenized samples were centrifuged at 3,000 rpm for 5 min at 4°C. The supernatant (cytoplasm protein) were harvested and the nuclear pellets were washed twice with buffer A (without NP-40) and resuspended in RIPA buffer, followed by 14,500 rpm for 5 min at 4°C. These samples were denatured by boiling in 1x SDS loading buffer for 5 min in 95°C and stored at −80°C for use.

Generation of Cell Lines with Stable Expression

Small Hairpin RNAs (shRNA) complementary to the N-terminal (GTCTTGTGTCCTTCAAATT) fragment of AURKA as described previously (Cai et al., 2012). pGIPz vector with luciferase target sequence (shLuc) was used as a control. The pGIPz vector containing shRNA sequence was co-transfected with lentivirus packaging plasmids (PSPA, and vesicular stomatitis virus G protein [VSVG]) into 293T cell by PEI method to generate lentivirus. The packaged viruses were used to transduce BCBL1 cells using 2 μg/ml of Puromycin. iSLK-Bac16 cells with AURKA knockdown were performed by transient transfection with AURKA shRNA. The RNA interference (RNAi) efficiency was assessed by quantitative PCR analysis. The pLVX-YFP vector containing AURKB-1-250, AURKB-77-344, AURKB-D76A and AURKB-WT was co-transfected with lentivirus packaging plasmid into 293T cell to generate lentivirus. These packaged viruses were used to infect BCBL1-luciferase and KMM-luciferase cells for stable expressing cells using flow cytometry.

Colony Formation and Cell proliferation assays

Plate colony formation assay was carried out as described previously (Jha et al., 2013). 3,000 and 1x10^4 iSLK-Bac16 or iSLK cells were seeded in a 100-mm^2 Petri plate and grown in 10% FBS contained DMEM with or without protease inhibitor (PMSF and Aprotinin). Medium was changed every three days. After 12 days of growth, the medium were discarded and cell were fixed with 4% formaldehyde and stained with 0.1% crystal violet. The plates were photographed by Canoscan LIDE 210. Soft agar colony formation assay was performed as described previously (Kakuguchi et al., 2010). Briefly, the bottom layer containing 0.75% agar in 10% FBS RPMI1640 were prepared first, and then the top layer contains appropriate amount of cells in 0.36% agar mixture were put on the bottom layer. The dish containing 2 layers was maintained in 37°C incubator for 3 weeks, and then the colonies were stained with 0.04% crystal violet-2% ethanol in PBS. For cell proliferation assays, a total of 6.25x10^5 BJAB, K-BJAB or

BCBL1 cells were seeded into 25cm^2 FLASK with 10 mL RPMI1640 medium and culture at 37°C. The cell numbers were counted using Vi-cell^{TM} XR (Becman coulter) at different time points.

Northern blotting

Total RNA were individually extracted from target cells by using TRIzol regent (Invitrogen) according to the manufacturer's Instructions. The quality of total RNA was evaluated by ratio of 28S/18S according to gel electrophoresis. A total of 20 μg total RNA was separated on 1% formaldehyde agarose gels and RNA was transferred onto nylon membrane. Specific RNA probe (AURKB-N-297bp, AURKB-C-302bp, ACTIN) were labeled in an vitro transcription reaction with digoxigenin-11-UTP using DIG Northern Starter Kit (Cat.No 12039672910 Roche), and membrane were hybridized with denatured DIG-labeled RNA probe overnight at 68°C with gentle agitation. After hybridization, the blots were washed and performed immunological detection. The chemiluminescent signal was detected by exposing to Bio-Rad image Lab device for 30 min.

KSHV virion purification and primary infection

iSLK-Bac16 cell were induced with 1 μg/ml Dox and 1mM sodium butyrate at 37°C With 5% CO_2 for 4 days when 90% of the cells were round and detached the plate. The virus supernatant were collected and spun down at 3,000 g for 15 min. Then the supernatants were filtered through 0.45 μm filter and virus particles were concentrated at 29,000 g at 4°C for 2h. The concentrated KSHV particles were resuspended in FBS contained complement medium and performed with primary infection. 0.5x10^6 HUVECs were seeded in 6-well plates 24 h before infection. Spin incubation (1,500 g, 1h, 25°C) were performed for KSHV infection. The samples were collected at day 1, 2, 3, and 5 after infection, respectively.

Tumor xenograft

Five-week-old female NOD/SCID mice with similar weight were randomly divided into 5 groups. Each mouse (9 mice/group) was individually injected intraperitoneally with 10x10^6 BCBL1-Luc cells carrying pLVX-vector, AURKB-WT, D76A, 77-344 or 1-250 in 200 μL PBS. The mice were subjected to live imaging at week 0, 3 and 5 post-inoculation. Live images were carried out as described previously with modification (He et al., 2017). The mice were intraperitoneally with D-luciferin at 150mg/kg body weight. Then the mice were imaged for 0.1 s, 0.5 s, 1 s, 5 s and 10 s at 12min after the injection of D-luciferin using an IVIS Spectrum Imaging System (PerkinElmer). Data were presented as total radiance within the ROI with mice imaged for 0.5 s.

QUANTIFICATION AND STATISTICAL ANALYSIS

Details of the statistical experiment can be found in each figure legends. Data are expressed as mean ± standard deviation (SD). Differences in mean between 2 groups were calculated using a two-tailed Student's t test. Statistical analyses were performed using GraphPad Prism software (version 5.0). Results from mouse survival experiments were analyzed with a log-rank (Mantel-Cox) test and expressed as Kaplan-Meler curves. For *in vivo* studies mice were assigned randomly to experimental arms. No statistical methods were used to establish sample size. Analysis of outcome was not performed in a blinded manner. A p value of < 0.05 was considered statistically significant and a p value of > 0.05 was considered statistically non-significant.

DATA AND SOFTWARE AVAILABILITY

All data are available upon request to the lead contact. No proprietary software was used in the data analysis. Raw data from Figures 1, 2, 3, 4, 5, 6, S1– S4, and S6 were deposited on Mendeley at https://doi.org/10.17632/s5d8fkzwhj.1.